IAMU
International Association of Maritime Universities

THE NIPPON FOUNDATION

International Association of Maritime Universities

IAMU 2022 Research Project
(No. YAS20220201)

A way to green voyage for LNG-fuelled ships : onboard Organic Rankine Cycle combined with Carbon Capture and Storage system

By

Shanghai Maritime university

August 2023

IAMU
International Association of Maritime Universities

This report is published as part of the 2022 Research Project in the 2022 Capacity Building Project of International Association of Maritime Universities, which is fully supported by The Nippon Foundation.

Published by the International Association of Maritime Universities (IAMU) Secretariat
Meiwa Building 8F, 1-15-10 Toranomon, Minato-ku,
Tokyo 105-0001, JAPAN
TEL : 81-3-6257-1812 E-mail : info@iamu-edu.org URL : http://www.iamu-edu.org

ISBN978-4-907408-47-3

IAMU 2022 Research Project
(No. YAS20220201)

A way to green voyage for LNG-fuelled ships : onboard Organic Rankine Cycle combined with Carbon Capture and Storage system

By
Shanghai Maritime university

Contractor : Jing Lu
Research Coordinator : Zhen TIAN

A way to green voyage for LNG-fuelled ships: onboard Organic Rankine Cycle combined with Carbon Capture and Storage system

Theme:Maritime transport for sustainable development

By

Shanghai Maritime university

Coordinator: Zhen TIAN

Associate Professor, Shanghai Maritime University, ztian@shmtu.edu.cn

Research partner: Wenzhong Gao

Professor, Shanghai Maritime University, wzgao@shmtu.edu.cn

Yuan Zhang

Associate Professor, Shanghai Maritime University, zhangyuan@shmtu.edu.cn

Chao Yang

Doctor, Shanghai Maritime University, yangc@shmtu.edu.cn

Hao Peng

Professor, Hainan University, 996027@hainanu.edu.cn

Haiyan Yu

Doctor, Shanghai Maritime University, yuhy@shmtu.edu.cn

Abstract The MEPC has called for 50% decarbonization from the shipping industry from 2008 levels by the end of 2050. In the context of this background, liquefied nature gas (LNG) is regarded as the most feasible fuel for ships. Before LNG burning in the dual-fuel engine, LNG needs to vaporize and overheat, during which about 860 kJ/kg cold energy would be discharged. On the other hand, about 50% of the fuel energy is lost as heat. Therefore, the efficient utilization of LNG cold energy and waste heat is of great significance to ship energy conservation and emission reduction. This report aims at exploring the feasibility of decarbonation for the LNG-fueled ships. The Carbon Capture and Storage (CCS) system is used to achieve the EEDI requirement in phase 3. Novelty, this work proposes the onboard organic Rankine cycle (ORC) combined with CCS to pursue the zero energy increasement for CCS. The ORC-CCS simulation model is established in Aspen HYSYS. Thermal and economic performances are studied under several different scenarios to reflect the circumstances in practice. The analyses of CO_2 emission reduction of LNG-fueled ship based on its economic feasibility are carried out. Moreover, a pilot-scale CCS is designed and manufactured. The results of this work would provide technical reference for improving energy efficiency and green shipping.

Keyword *LNG-fueled ships, Green voyage, Organic Rankine Cycle, Carbon Capture and Storage, EEDI*

Executive Summary

This project aims at improving ship energy efficiency, reducing CO_2 emission and fulfilling green voyage. The details include:

- Recovering cold energy and waste heat of LNG-felled ships via Organic Rankine Cycle (ORC).
- Investigating the feasibility of onboard Carbon Capture and Storage (CCS) system.
- Analyze the configuration of the ORC-CCS for the reference ship.
- Providing support material for the EEDI revision for LNG-fueled ships.

To achieve the four objectives, we conduct a systematic literature review and the possibility of LNG cold energy and waste heat recovery is theoretically analyzed. Based on the guideline of EEDI, the amount of CO_2 reduction is determined, which provide the design instructions for the ORC-CCS system. Furthermore, a refence ship is selected for ORC-CCS system design and modelling development from two aspects. Firstly, the onboard CCS is designed and numerically studied from thermo-economic aspect. Secondly, the combined ORC-CCS is simulated and analyzed from energy, exergy and economic perspective with the variation of working parameters. At last, a pilot scale CCS system is designed and manufactured.

The main finds of this project are as follows. The EEDI requirement for the reference ship is calculated and the CO_2 reduction for meeting the EEDI phases is determined. The LNG cold energy could be utilized for ORC power generation and CO_2 capture. It concludes that the LNG cold energy utilization technologies are relatively mature, and they have been widely adopted in the onshore conditions. A Kamsarmax vessel is taken as an example and the plasticity of the system is analyzed from three perspectives: energy, exergy and economic via Aspen HYSYS. The CCS optimum operating parameters are m_{exh}=20000 kg/h, m_{sol}=16000 kg/h. The amount of CO_2 captured at this point is 760.4 kg/h, which is well above EEDI Stage 3 requirements. The total initial cost of CCS is 1.38 million US $. Under the designed working conditions, the ORC system can generate enough electricity to fully meet the system's electricity demand. The maximum power generated by the ORC is 123.7 kW and CO_2 capture rate also reaches 78.64%. Meanwhile, the system exergy efficiency increases from 19.59% to 28.03%. Increasing the exhaust gas flow rate will increase the amount of captured CO_2, but there is an upper limit to the capture amount. When the solution flow rate is 21000 kg/h and the exhaust gas flow rate is 20000 kg/h, the maximum amount of captured CO_2 is 1686 kg/h. As the CO_2 capture amount changes slowly and the regeneration heat changes significantly with the solution, the specific reboiler duty also increases from 4.62GJ/tonCO_2 to 4.71GJ/tonCO_2. The equipment capital investment is mainly from the heat exchanger, which accounts for 48.5%.

In our research, the results are consistent and convincing. For the future research, there is a need to investigate the details of different ship types to generate a universal guideline for EEDI revision. Also, the dynamic simulation and experimental validation of the proposed system should be carried out. All these point out the potential direction for the near future research.

The research deliverables also include:

We shared two presentations for the AGA 22 titled “Feasibility study on carbon capture system of LNG-fueled ship based on comprehensive utilization of heat and cold energy” and “A way to green voyage for LNG-fueled ships: onboard Organic Rankine Cycle combined with Carbon Capture and Storage system”. The conference paper has been published on “22nd Annual General Assembly of the International Association of Maritime Universities Conference, AGA IAMUC 2022”.

We have submitted two talks to AGA 23, including Paper 1 titled “A Zero Energy Increment Onboard Carbon Capture System for LNG-fueled Ship” and Paper 2 titled “Thermo-economic analysis on OCCS of LNG dual-fuel vessels based on the EEDI framework”.

1. Introduction

1.1 Background

In October 2016, the Maritime Environmental Protection Committee (MEPC) of the International Maritime Organization (IMO) adopted the resolution MEPC.280 (70), namely Sulphur Limit Order 2020. Sulphur content in ship fuel needs to be reduced from 3.5% to less than 0.5% by January 2020 [1]. Meanwhile, the MEPC has called for 50% decarbonization from the shipping industry from 2008 levels by the end of 2050. Although there are increasing energy conservation and emission reduction technologies, studies that address the green and zero-carbon ships are still at the beginning stage and are far behind other industries, such as zero-carbon buildings.

Compared with heavy oil, the Liquefied Natural Gas (LNG) can reduce SOx by 90%, NOx by 80%, CO_2 by 20%, and particulate matter by 100%[2]. With the improvement of global refuelling vessel layout and the development of dual-fuel engines, LNG-fuelled ships have developed from small river vessels to large ocean vessels. The number of LNG-fuelled ships in service is shown in Fig. 1-1. According to Sharples, the number will be doubled by 2026 and will account for 32% of the total ship demand by 2050[3].

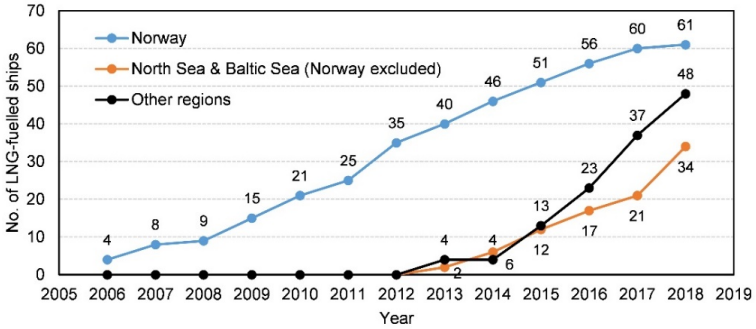

Fig. 1-1 LNG-fuelled ships in service (source: DNV GL)

More stringent emission regulations make the focus shift from energy efficiency improvement to CO_2 reduction. In recent years, the Carbon Capture and Storage (CCS) has attracted researcher's attention. LNG, to some extent, could be treated as clean fuel except for the CO_2 emission. To overcome this shortage, post combustion CCS for dealing with the tail gas is mostly recommended. As for the CCS, the alcohol-amine-based absorption method has become the main decarbonization method because of the characteristics of high absorption load, recyclable absorbent and low cost. Inspired by the cryogenic cold energy and waste heat, the feasibility of the onboard carbon capture system (OCCS) attracts attention. With the OCCS, the CO_2 contained by the exhaust gas would be captured and concentrated. For the convenience of storage and transport, the gaseous CO_2 is liquified and transported to the port for commercial utilization.

LNG-fuelled ships release a large amount of LNG cold energy and main engine waste heat at the same time during sailing, which provides a key condition for realizing zero-consumption CO_2 capture and storage. Some progress and accumulated experience have been made in the utilization of LNG cold energy. The ORC synergistic CO_2 capture for LNG-fuelled ships has not yet been integrated into a complete system. Therefore, it is essential to study the zero-emission LNG-fuelled ship based on the ORC-CCS system.

1.2 Objectives

Low carbon shipping and improved air quality are driven by a combination of improvements in the Energy Efficiency Design Index (EEDI) and the use of alternative fuels. This project is aimed at improving energy efficiency, reducing CO_2 emission and fulfilling green voyage. Therefore, the cold energy and waste heat of LNG-fuelled ships would be recovered with the Organic Rankine Cycle (ORC). Additionally, the feasibility of OCCS system would be investigated.

The research questions of this project mainly include: (1) To clarify CO_2 emission of LNG-fuelled ships under different operation strategies. (2) To investigate the feasibility of the onboard CCS and zero-carbon ship. (3) Design and performance analysis of onboard ORC-CCS based on LNG cold energy recovery. For this, detailed thermo-economic modelling would be and established, and the performance analysis would be approached. (4) To provide support material for the EEDI revision for LNG-fuelled ships. The innovation of energy-efficient utilization technology for ships would be promoted. Moreover, the research results of this project would lay the foundation of convention amendment and facilitate green voyage.

1.3 Methodology and Outputs

According to the research objectives, this project is broken down into four packages. The packages and the methodologies are shown in Fig. 1-2.

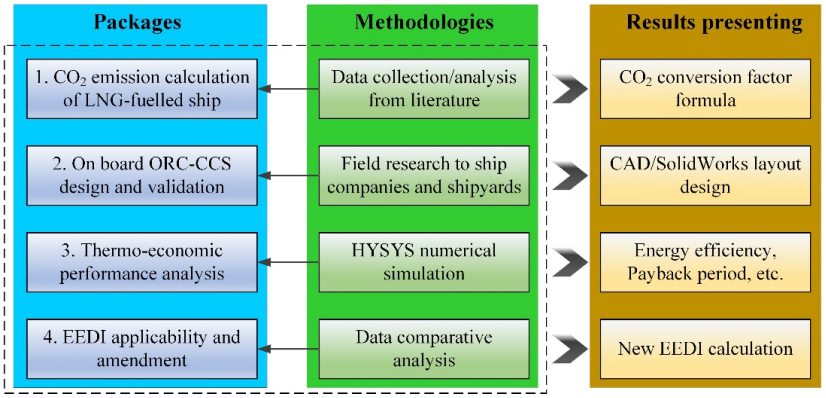

Fig. 1-2 Flow chart of the research methodologies

1.4 Report Outline

The report consists of 7 Sections.

Section 2 briefly introduces EEDI guidelines and LNG-fuelled ship energy recovery. Also, the reference ship for latter analysis is presented. Section 3 is devoted to the literature review for LNG cold energy utilization. Based on the afore 2 sections, Section 4 gives the detail on the design of onboard carbon capture and storage system. The thermo-economic analyses are carried out. Later on, the design of the onboard organic Rankine cycle combined with carbon capture and storage (ORC-CCS) system is described in Section 5. The ORC-CCS for achieving zero energy increasement CCS is validated theoretically. Section 6 contains the recommendations concerning application of the ORC-CCS. Section 7 details final conclusions.

2. EEDI guidelines and LNG-fuelled ship energy recovery

2.1 EEDI guidelines

The Energy Efficiency Design Index (EEDI) is a measure of the level of CO_2 emissions inherent in the design and construction phase of a ship, which represents the amount of CO_2 emitted per ton/mile of the ship. The EEDI is established to constitute a minimum standard of energy efficiency for new built ships in the future. A baseline of emissions is established through statistical analysis of existing vessels of various types and tonnages, based on which the energy efficiency of newbuilding ships could be controlled. With respect to the EEDI, the attained EEDI and the required EEDI are generally discussed. After the implementation of the EEDI, the attained EEDI of newly built ships of all types and different tonnages must be smaller than the required EEDI.

The EEDI is divided into 3 stages, the specific requirements of which are as follows:

(1) Phase I: Effective from January 2015, all newbuilding ships will be required to reduce their carbon emissions by 10% from the baseline standard.

(2) Phase II: Effective from January 2020, all newbuilding ships will be required to reduce their carbon emissions by 20% from the baseline standard.

(3) Phase III: Effective January 2025, all newbuilding ships will be required to reduce their carbon emissions by 30% from the baseline standard. The EEDI Phase III effective date for gas carriers, cargo ships and LNG carriers has been brought forward from January 2025 to April 2022, and the EEDI reduction rate requirement for some ship types has been increased.

Therefore, we are in Phase III of the EEDI. More details could be found in the MEPC.1/Circ.896 [4]. EEDI requirement is determined by the ship type and size. The required EEDI Cut-off levels, phases and reduction rates are summarized in Table 2-1. In our work, the Bulk carrier is focused.

Table 2-1 Required EEDI Cut-off levels, phases and reduction rates

Ship Type	**Size**	**Phase 1** 2015.1.1-2019.12.31	**Phase 2** 2020.1.1-2024.12.31	**Phase 3** 2025.1.1~
Bulk Carriers	**20000 DWT and above**	**10**	**20**	**30**
	10000-20000DWT	**0-10***	**0-20***	**0-30***
Gas Tankers	10000DWT and above	10	20	30
	2000-10000DWT	0-10*	0-20*	0-30*
Tankers	20000DWT and above	10	20	30
	4000-20000DWT	0-10*	0-20*	0-30*
Container ships	15000DWT and above	10	20	30
	10000-15000DWT	0-10*	0-20*	0-30*

The Required EEDI for Bulk carrier is calculated with the reduction factor X in different phases, as shown in Eq. (2-1).

$$Requireed\ EEDI = (1 - X/100) \times RLV \tag{2-1}$$

Where, RLV indicates Reference Line Value, RLV for bulk carriers are as shown in Table 2-2.

Table 2-2 RLV for bulk carriers

Vessel type	DWT	*RLV* calculation formula
Bulk carriers	≤279000t	$961.79\times DWT^{-0.477}$
	>279000t	$961.79\times 279000^{-0.477}$

The Required EEDI for bulk carriers are shown under different phases in Fig. 2-1.

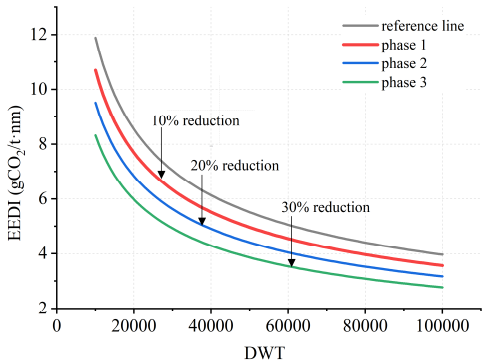

Fig. 2-1 Required EEDI for bulk carriers under different phases

The Attained EEDI for the ship is a measure of the level of energy efficiency of a ship and is calculated as follows:

$$Attained\ EEDI = \frac{(\prod_{j=1}^{n} f_j)(\sum_{i=1}^{nME} P_{ME(i)} \cdot C_{FME(i)} \cdot SFC_{ME(i)}) + (P_{AE} \cdot C_{FAE} \cdot SFC_{AE}) + \{(\prod_{j=1}^{n} f_j \cdot \sum_{i=1}^{nPTI} P_{PTI(i)} - \sum_{i=1}^{neff} f_{eff(i)} \cdot P_{AEeff(i)})C_{FAE} \cdot SFC_{AE}\} - (\sum_{i=1}^{neff} f_{eff(i)} \cdot P_{eff(i)} \cdot C_{FME} \cdot SFC_{ME})}{f_i \cdot f_c \cdot f_l \cdot Capacity \cdot f_w \cdot V_{ref} \cdot f_m} \quad (2\text{-}2)$$

Where, *ME* and *AE* denote main and auxiliary machines respectively; *i* stands for number of engines; *P* stands for power which measures in *kW*; C_F stands for carbon conversion factor, it is a dimensionless factor that converts fuel consumption into CO_2 emissions based on its carbon content, and which measures in *t*-CO_2/*t*-*Fuel*; *f* stands for fuel consumption parameter, it refers to the approved unit fuel consumption of a diesel or steam turbine, measured in *g/kWh*; *f* is the various correction factors related to the ship type, all taken as 1 in this paper; *Capacity* stands for the deadweight tonnage of the vessel, measured in *t*; V_{ref} refers to the speed of a ship in deep water under assumed windless and wave-free meteorological conditions, measured in *knot*; the *PTI* section calculates the CO_2 emissions from shaft motor assisted propulsion ; the *EFF* section is a calculation of the CO_2 emission reductions resulting from the adoption of innovative energy efficiency technologies. To obtain the specific values of the EEDI, the reference ship should be introduced.

2.2 Reference ship

Unlike conventional ships, the LNG-fuelled ship carrying the dual-fuel (DF) engine, which can switch between oil and gas modes. A large amount of waste heat produced by the DF engine is released into the environment. The energy balance of a typical four-stroke turbocharged DF engine is shown in Fig. 2-2, which demonstrates that about 50% of the fuel energy is lost as heat. Therefore, the efficient utilization of waste heat is of great significance to ship energy conservation and emission reduction.

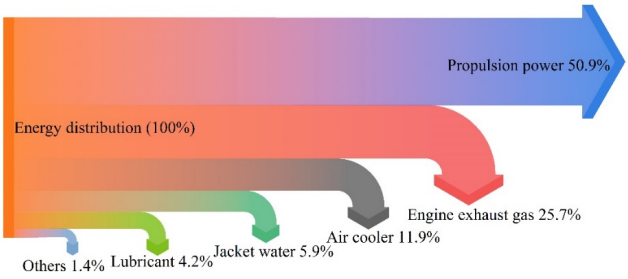

Fig. 2-2 The energy balance of a dual-fuel engine

This paper selects a typical Kamsarmax ship with a dual-fuel main engine (Wärtsilä 12V50DF) as the reference ship, which are demonstrated in Fig. 2-3 and Fig. 2-4. The detailed parameters of the reference ship are shown in Table 2-3. LNG fuel is stored in tanks at a pressure of 100 kPa and a cryogenic temperature of -162°C, the engine requires natural gas to have inlet temperature of 60°C and a pressure of 600kPa. The composition of exhaust gas is 75wt% N_2, 16.6wt% O_2, 4wt% H_2O and 4.4wt% CO_2. The parameters of LNG to engine and exhaust gas from engine are shown in Table 2-4 and Table 2-5.

Fig. 2-3 The references ship-Kamsarmax ship

Table 1-3 Main specifications of reference ship

Parameter	Value	Parameter	Value
Type	Bulk	LNG tank	600 m^3
Ship length overall	229 m	Heavy oil tank	1800 m^3
Ship beam	32 m	Marine diesel oil tank	400 m^3
Deadweight	81190 DWT	Main engine type	Wärtsilä 12V50DF
Reference speed	14 knots	MCR rating of main engine	9930 kW

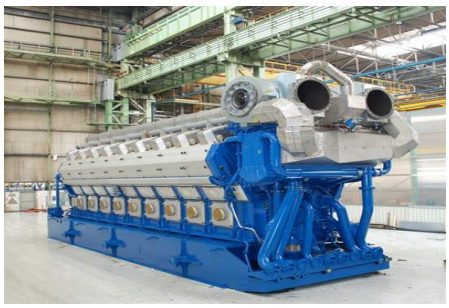

Fig. 2-4 The dual fuel engine Wärtsilä 12V50DF

Table 2-4 LNG data for Wärtsilä 12V50DF engine

Engine load	**100%**	**75%**	**50%**
Mass flow rate (kgh^{-1})	2196	1728	1260
Cold energy released (kW)	602.4	474	345.6
Available cold energy per kg CO_2 ($kWhkg^{-1}$)	0.18	0.19	0.20

Table 2-5 Exhaust gas data for Wärtsilä 12V50DF engine

Engine load	**100%**	**75%**	**50%**
Mass flow rate (kgh^{-1})	68400	52560	41040
CO_2 concentration (%)	4.8	4.6	4.2
CO_2 production (kgh^{-1})	3283.2	2417.8	1723.7
Inlet temperature (℃)	383	303	285
Outlet temperature (℃)	120	120	120
Heat in exhaust gas (kW)	3106.3	2679.8	1886.6
Available heat per kg CO_2 ($kWhkg^{-1}$)	0.95	1.11	1.09

2.3 EEDI for the reference ship

This study uses Ψ to reflect the captured CO_2 via the OCCS. Thus, ψ could be calculated from Eq. (2-3). The proposed factor ψ provides suitable criteria for OCCS design. The required EEDI, attained EEDI and the CO_2 captured by OCCS are summarized in Table 2-6.

$$Required\ EEDI\left(gCO_2/ton.nm\right) = Attained\ EEDI - \frac{\Psi/1000}{f \cdot Capacity \cdot V_{ref}} \tag{2-3}$$

Table 2-6 Attained EEDI and required EEDI for the reference ship.

	Phase 0	**Phase 1**	**Phase 2**	**Phase 3**
Attained EEDI ($gCO_2(tn \cdot m)^{-1}$)			3.61	
Required EEDI ($gCO_2(tn \cdot m)^{-1}$)	4.38	3.94	3.51	3.07
Ψ (kgh^{-1})	---	---	113.7	613.8

2.4 Summary

In this chapter, the EEDI guidelines are briefly introduced. Additionally, a typical Kamsarmax ship with a dual-fuel main engine is selected as the reference ship. The EEDI requirement for the reference ship is calculated and the CO_2 reduction for meeting the EEDI phases is determined. Also, the reference ship would provide the critical boundary conditions for the design of the onboard carbon capture system.

3. LNG cold energy utilization and CO_2 capture

3.1 LNG cold energy releasing characteristics

Natural gas (NG), as the intermediate substitute between traditional and renewable energy, plays an increasingly important role in economy development [5][6]. Liquid natural gas (LNG) is an effective way in the global energy market due to easy transportation and high energy density [7]. According to the International Gas Union, global LNG trade reached 482 billion cubic meters in 2018, with an annual growth rate of 13% [8]. The NG uneven distribution facilitates LNG transportation by sea [9]. Fig. 3-1 shows the global distribution of the major liquification and regasification stations in the world, as well as LNG maritime transportation routes [10].

Fig. 3-1 Map of worldwide distribution of LNG plants and maritime trade routes [11]

Before LNG could be utilized by the end-users, it requires to be vaporized in the regasification stations by the heat sources, such as seawater and air [12]. If so, most high-grade cold energy of LNG would be wasted. During the regasification process, approximately 830 kJ/kg cold energy would be released when LNG temperature rises from -162 °C to 25 °C [13, 14]. Since the temperature of the cryogenic fluids is far lower than the normal temperature, it is considered as high quality “cold energy”. The LNG vaporization process is divided into three temperature ranges: the liquid area, the two-phase are and the vapor area. The LNG would first undergo a steep heating process, in which the LNG is gradually heated to the bubble point temperature. Then, the LNG enters the phase transition process, where LNG absorbs a great deal of latent heat and vaporizes to NG. Finally, NG enters the superheated vapor area, and it is heated to the user's required temperature.

The vaporization pressures have a great influence on the regasification characteristics of LNG. When the pressure is low, the dew point temperature of LNG is also low, and there is still a lot of cold energy after the complete vaporization into NG. As the pressure increases, the dew point temperature gradually increases, releasing a large amount of cold energy before the LNG vaporizes. Therefore, the influence of regasification pressure should be fully considered in the design of system parameters, and the reasonable segmentation utilization of LNG cold energy should be carried out according to different conditions. Fig. 3-2 shows the temperature entropy diagram (*t-s*) of LNG vaporization process under different pressures. The cold energy releasing characteristics are demonstrated in Fig. 3-3.

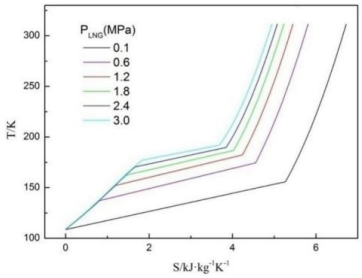

Fig. 3-2 Temperature entropy diagram (*t-s*) of LNG under different pressures

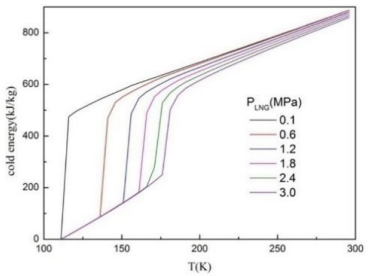

Fig. 3-3 LNG cold energy releasing characteristics

As for power generation utilizing cold energy, the physical exergy of LNG is mainly recovered. The chemical reaction exergy and diffusion exergy are not included. The physical exergy mainly includes thermal exergy and pressure exergy. Therefore, according to the utilization of physical exergy, there are two types of power generation: thermal exergy power generation and pressure exergy power generation. At ambient temperature T_0, the available thermal exergy and pressure exergy are expressed as:

Thermal exergy,

$$\begin{aligned} ex_r &= c_p(T-T_0) + T_0\int_{T_0}^{T}\frac{\delta_q}{T} \\ &= c_p(T-T_0) + c_pT_0\ln(T_0/T) \end{aligned} \tag{3-1}$$

Pressure exergy,

$$ex_p = T_0R\int_{P_0}^{P}\frac{\delta_q}{P} = T_0R\ln(p/p_0) \tag{3-2}$$

When the regasification pressure is lower than 6.68MPa, LNG is under the subcritical evaporation. When the LNG regasification pressure is 0.6MPa, the thermal exergy between the two-phase region accounts for 78.9%, while that in the vapor-phase region only accounts for 3.6%. Therefore, the thermal exergy recovery should focus on the liquid-phase region and the two-phase region when LNG is subcritical regasification.

Table 3-1 LNG thermal exergy distribution in different regions under 0.6 MPa [15]

Parameters	Liquid region	Liquid-vapor region	Vapor region	Total
Temperature (℃)	-161.8~-133.6	-133.6~-54.9	-54.9~5.0	-161.8~5.0
Thermal exergy (kJ/kg)	125.3	564.6	25.8	715.8
Proportion (%)	17.5	78.9	3.6	100.0

3.2 LNG cold energy utilization

The LNG is stored at a low temperature of -162°C and needs to be regasified before entering the DF engine, which will release about 830 kJ/kg cold energy [16]. Recovering LNG cold energy is of great significance to improve energy utilization efficiency. Many LNG cold energy recovery methods have been developed over the past decades, such as power generation[17, 18], cold storage [19], and air separation [20]. In recent years, the utilization of LNG cold energy for CO_2 capture [21], seawater desalination [22], and light hydrocarbon separation [23] has gradually become the mainstream trend. A comprehensive review of LNG cold energy recovery could be found in He et al.'s work [24], which provides the suggestions and directions for the high-efficient LNG cold energy recovery. Considering the large temperature range, many researchers suggest to reduce the irreversible loss through energy cascade utilization [25]. Fig. 3-4 illustrates the methods of utilizing LNG cold energy within different temperature zones. Among various utilization methods, the Organic Rankine Cycle (ORC) for power generation occupies the widest operating temperature range.

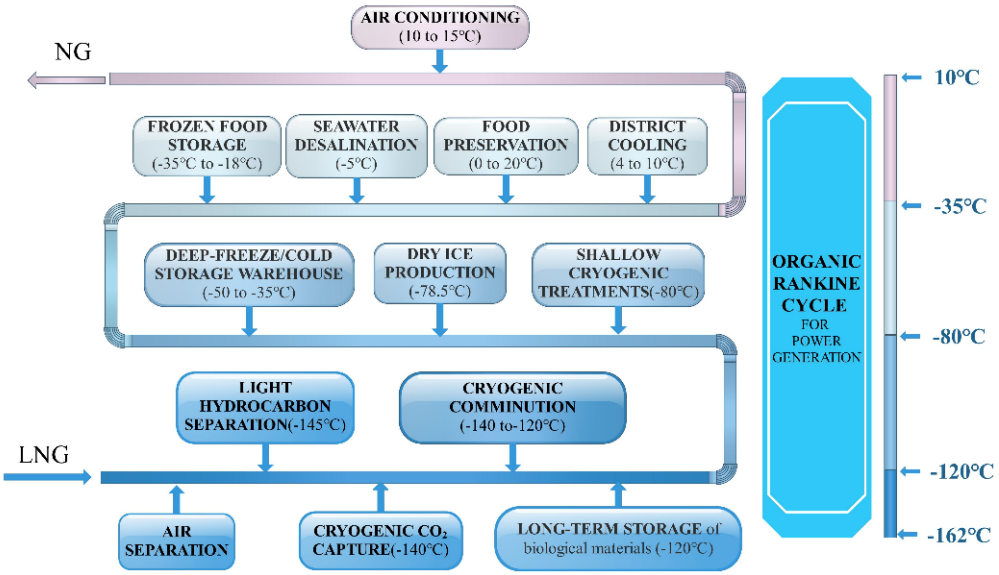

Fig. 3-4 LNG cold energy utilization methods within different temperature zones

3.3 ORC based on LNG cold energy recovery

The organic Rankine cycle (ORC) has sparked interest in waste heat utilization since the 19th century [26]. Besides solar energy [27], geothermal energy [28], ocean thermal energy [29] and other low-grade heat sources, the application of ORC has penetrated the cryogenic field. The cryogenic cold energy released during the regasification process is recommended as an optimum heat sink for ORCs. LNG cold energy has been extensively used in power generation from the past to the present. Moreover, the practical feasibility is validated since the ORC converts high-grade LNG cold energy into high-grade electricity [30-32]. The investigations of the ORC topics focus on the structure [33], working medium [34], and operation strategy [35]. Choi et al. [36] compared five structures of ORC systems recovering LNG cold energy. It should be noticed that when construct the ORC system, the ORC system structure needs to be combined with the LNG cold energy release principle. If LNG is used as the cold source in a single-stage Rankine cycle power generation system, the heat transfer temperature difference will be large. The multi-stage ORC is an important direction for performance improvement. The use of multi-stage condensation in the thermal cycle can improve the heat transfer characteristics between the LNG

and the working medium and improve the efficiency of the power generation system. Bao et al. [37] proposed a two-stage ORC system using propane as the working medium. Compared with the traditional ORC systems, the net power output, energy efficiency, and exergy efficiency of the system were increased by 45.27%, 42.91%, and 52.31%, respectively. Xue et al. [38] presented a two-stage ORC, by which the low-grade heat of exhaust flue gas combined cycle power generating unit, as well as the cryogenic energy of LNG could be effectively recovered and utilized. Jamali and Yari [39] simulated the performance of a novel ORC designed between LNG and concentrated photovoltaics, which could generate 24.4 MW of power and supply 223 kg/s of cooling water. In the work of Joy and Chowdhury [40], a cascaded three-stage ORC with ethane, propane and ethane as working fluids was established, which could produce an additional power of 100 kW when using the cryogenic heat sink. Tian et al. [41] constructed a two-stage parallel ORC for a LNG-fueled ship to utilize cryogenic cold energy. In their study, the working medium mass fraction and the pinch point temperature difference were investigated. He et al. [42] provided theoretical principles for cryogenic ORC working fluids selection. In the work of Choi et al. [43], R290 was suggested as the optimum working fluid to achieve maximum power. Mosaffa and Farshi [44] explored the enhancement of the cryogenic ORC performance by adding solar energy utilization. The results indicated that the system generated 95.67 MJ/(m^2year) of power with an energy efficiency of 3.28%. Recently, the combined cryogenic ORC with carbon dioxide capture [45], light hydrocarbon separation [46], and data center cooling [47] have been proposed to explore more possibilities.

With regards to the design of ORC architectures, multi-stage ORC systems have been proposed based on energy cascade utilization. Besides the basic ORC (bORC), the two-stage ORC including series two-stage ORC (stORC) and parallel two-stage ORC (ptORC) are widely used. As early as in the year of 2015, Lecompte et al. [48] presented a review work focused on the ORC architectures for waste heat recovery. Some barriers to the ORC development were pointed out. Recently, Marandi et al. [49] proposed a ptORC for stack waste heat recovery from fuel cell, the energy and exergy efficiencies for the overall system were observed to be 58.15% and 36.64%, respectively. Li et al. [50] compared the thermal-economic performances of the bORC and the stORC. They found the only advantages of stORC in the net power output and the exergy efficiency, but no benefits in the energy efficiency. Meanwhile, the economic advantages of the bORC were proved. Surendran and Seshadri [51] investigated the thermal performances of the stORC, ptORC, and pre-heated bORC. Compared with the pre-heated bORC, the stORC delivered 8.5% increase in the output power, while the output power of ptORC decreased by 0.3%. The research results of Braimakis et al. [52] showed that the double-stage ORC had higher exergy efficiency by up to 50.5% compared to the bORC. Even though some performance indicators could be improved via increasing ORC stages, the system complexity and the investment are still the challenges for the manufacturers.

From an engineering practice point of view, improving the energy efficiency of the bORC is more favored. As for the bORC, the recuperative ORC (rORC) via adding a recuperator or regenerator is regarded as the most promising method [53-55]. The schematics of the ORC with recuperator and regenerator are illustrated in Fig. 3-5 and Fig. 3-6, respectively. In these two cases, the working medium is preheated before entering the evaporator, but the working principles are different. In the rORC with a recuperator, the working medium is preheated by the remaining heat at the expander outlet [56]. In the rORC with a regenerator, the working medium is heated by the superheated vapor extracted from the intermediate expansion stage [57]. After that, the subcooled liquid and vapor streams are mixed in the heater. Mosaffa et al. [58] carried out thermo-economic analysis for the rORCs for recovering liquid natural gas (LNG) cold energy and geothermal energy. They suggested that the rORC with a recuperator achieving the maximum exergy efficiency of 39.93% was preferable compared to the other architectures.

Mehrpooya et al. [59] performed the thermo-economic analysis for a recuperative two-stage ORC driven by solar energy and LNG cold energy, which led to 35.66% increase in energy efficiency compared with the bORC. In the work of Imran et al. [60], the thermal efficiency and specific investment cost of the bORC, single-stage rORC, and double-stage rORC were optimized. However, the results demonstrated that the single-stage and double-stage recuperator ORCs could slightly increase the thermal efficiency of 1.01% and 1.45%, respectively. Meanwhile, the specific cost was increased to 187 $/kW and 297 $/kW, respectively. Therefore, it is necessary to comprehensively evaluate the performances of the single-stage rORC.

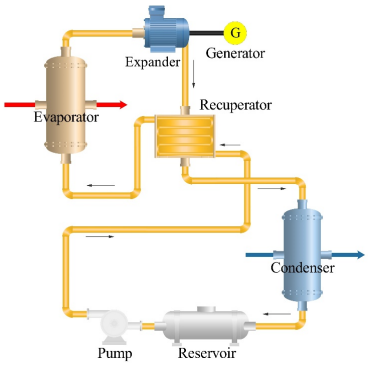

Fig. 3-5 Schematic of the recuperator ORC

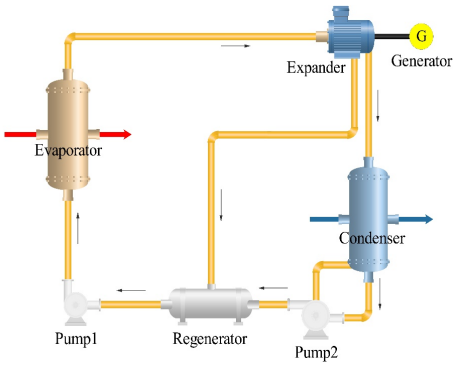

Fig. 3-6 Schematic of the regenerator ORC

To improve the energy efficiency, several researchers have carried out studies on the ORC based on ship waste heat recovery (WHR). Choi and Kim [61] studied a two-stage ORC suitable for recovery of engine exhaust gas (EEG) waste heat of 6800TEU container ships, and the propulsion efficiency of the engine was increased by 2.824%. Lee and Choi [62] compared three ORCs with different structures to recover LNG cold energy and waste heat from the floating power platform. The results showed that the two-stage ORC with seawater and EEG as heat sources had the largest output power. Soffiato et al. [63] utilized jacket cooling water (JCW), air cooler, and lubricating oil as heat sources and obtained a two-stage ORC suitable for LNG carriers by optimizing the system structure. Sung and Kim [64] established a two-stage ORC for the cold energy and waste heat of the LNG dual-fuelled ship, using EEG and JCW as heat sources. The results demonstrated that the net power output was increased by 906.4kW by using preheater and regenerator, which was 5.17% higher than that of the original system. Tian et al. [65] proposed a series and parallel combined ORC based on LNG cold energy and waste heat of DF engine

with JCW and EEG as parallel heat sources. The output power range was 199.97~218.51kW, the energy efficiency range was 13.64%~15.62%, and the exergy efficiency range was 25.29%~27.3%. Sun et al. [66] established a three-stage ORC power generation system model based on a 100,000-load LNG-fuelled ship. The results showed that the maximum power generation was 457.41kW/kgLNG. The maximum thermal efficiency and exergy efficiency of the system were 35.56% and 48.06%, respectively.

3.4 CO_2 capture with LNG cold energy recovery

Meanwhile, the LNG cold energy used for CO_2 capture has been widely investigated because of the huge potential of carbon capture in energy and commercial value [67]. Zhao et al. [68] proposed a novel combined system with a twin-stage ORC power generation and CO_2 capture using LNG cold energy and waste heat from the magnesite processing industry. Their system could reach the exergy efficiency of 0.57 and provide 119.42 kW electric power and liquid CO_2 of 0.75 t/ton LNG. Gómez et al. [69] proposed an innovative power plant with LNG exergy utilization and the capture of CO_2 proceeding from the flue gases. As a result, a high efficiency exceeding 65% was achieved, with almost zero greenhouse gas emission. Mehrpooya et al. [70] developed an integrated coal gasification process with a novel double-column cryogenic air separation unit based on the LNG cold energy recovery. The outlet LNG stream from air separation unit was utilized as cold source of the condenser in the trans-critical CO_2 power cycle. The results demonstrated that 99.83% of CO_2 with 99.80% purity was captured and the required power was around 0.10 kWh/kg CO_2. Aghaie et al. [71] introduced an integrated system combining biomass gasification, chemical looping hydrogen production, CO_2 capture, solid oxide fuel cell system, and a steam power cycle, which generated the system net efficiency of 55.8% with 100% CO_2 capture. Based on the LNG cold energy and waste heat from solid oxide fuel cell, Liu et al. [72] proposed a combined system. The results illustrated that the net power generation efficiency was about 79.81% and the CO_2 capture rate was 79.2 kg/h under the given conditions. A zero-CO_2 emission high-efficiency power cycle using LNG cold energy was designed and analysed by Liu et al [73]. Wang et al. [74] used LNG cold energy to capture CO_2 in the flue gas of the magnesite processing industry, and the results showed that the utilization rate of LNG cold energy and CO_2 capture amount reached 20.81% and 0.29t/tLNG, respectively. Pan et al. [75] established a combined system of Kalina and ORC for CO_2 capture with the capture amount of 0.6t/tLNG. Xu and Lin[76] carried out a similar study. Bao et al. [77] used LNG cold energy to capture CO_2 after combustion of the natural gas power plant. The system efficiency was increased by 2.51%, and the efficiency loss was reduced to 7.9%. However, the application of LNG cold energy to liquefy CO_2 in maritime technology is still in its early stage. Feenstra et al. [78] studied the feasibility of onboard CCS. The analysis results showed that the cost of liquefied CO_2 using LNG cold energy was 233~323€/t.

The research on the alcohol-amine-based absorption OSSC has been widely studied. Seo et al. [79] developed several CO_2 liquification processes and evaluated the availability of the ship-based CCS from a life cycle cost perspective. Feenstra et al. [78] investigated the feasibility of ship-based CCS on a cargo ship. 30 wt% aqueous monoethanolamine (MEA) and 30 wt% aqueous piperazine (PZ) were used as solvents. The carbon capture cost was in the range of 98 to 389 €/tCO_2. Fang et al. [80] proposed an optimal sizing model to determine the capacity of the shipboard CCS. They pointed out that a 6MW OCCS could reduce124 tons CO_2, which was 55.8% of the total shipping GHG emission. Long et al. [81] developed a system using MEA/PZ and MDEA/PZ as solvents for CO_2 capture, compression and liquefaction onboard a 3000 kW diesel engine. The results demonstrated that CO_2 removal could be up to 1348 kg/h under the optimum configuration. Ros et al. [82] designed a ship-based CCS considering solvent selection, heat integration and ship movement. The techno-economic analyses showed that the cost of CO_2 capture for the Sleipnir varied within 119-133 €/tCO_2. Einbu et al. [83] alleged that the

waste heat recovered from the engine exhaust gas was not sufficient for the demand of an absorption-based CCS operating 50% capture rate with 30 wt% MEA as solvent. From the literature review, even though the waste heat from the exhaust gas has been widely applied in OCCS, the utilization of cryogenic cold energy released by the LNG regasification process is seldomly reported.

3.5 Summary

In this chapter, the LNG cold energy releasing characteristics are firstly presented. Then, the literature review for LNG cold energy utilization has been addressed. In particular, the LNG cold energy could be utilized for ORC power generation and CO_2 capture. It concludes that the LNG cold energy utilization technologies are relatively mature, and they have been widely adopted in the onshore conditions. The application scenarios include the LNG receiving station, LNG power plant, etc. However, as for the onboard LNG cold energy utilization, few works are reported. Therefore, the onboard ORC and CO_2 capture system for achieving green voyage.

4. Onboard Carbon Capture and Storage system

4.1 Design of Onboard Carbon Capture and Storage system for LNG fuelled ship

The OCCS aims at capturing CO_2 from the engine exhaust gas of the LNG-fueled ship. The captured CO_2 is compressed and liquified before being stored in the tank. The liquified CO_2 would be further transported to a chemical plant for utilization or to an underground injection site for permanent storage. The content of CO_2 in the exhaust gas of diesel or LNG is usually no more than 5 vol%. Therefore, CO_2 separation from the exhaust gas and concentration improvement is the first step for further treatment. CO_2 separation and capture need significant energy input. Ideally, the waste heat from the ship engine exhaust gas should be considered. The electricity consumed by the compressor comes from the ship as well. Compared with the waste heat, the applicable cold energy is much smaller. Therefore, the capacity of OCCS is limited by the cold source conditions. As for the CO_2 liquification process, the cryogenic temperature is required. Considering the temperature range, the LNG cold energy is used for the concentrated CO_2 cooling and liquification. The supplementary cold energy is provided by the seawater. Fig. 4-1 illustrates the block diagram of the overall concept design of the OCCS. The Inputs and outputs for each block of OCCS are summarized in Table 4-1.

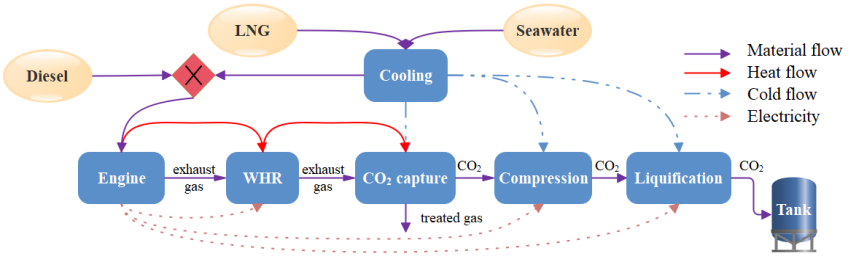

Fig. 4-1 The block diagram of the overall concept design of the OCCS.

Table 4-1 Inputs and outputs for each block of OCCS

Block	Inputs	Outputs
Main Engine	Fuel type (LNG or MDO)	Fuel consumption (kgh^{-1})
	Engine load (kW)	Flue gas temperature (°C)
		Flue mass flow rate (kgh^{-1})
		CO_2 content (wt%)
Waste heat recovery (WHR)	Flue gas inlet temperature (°C)	Heat recovery amount (kW)
	Flue mass flow rate (kgh^{-1})	Flue gas outlet temperature (°C)
	Heat capacity demand from CO_2 capture (kW)	
CO_2 capture	Solvent concentration (wt%)	Solvent mass flow rate (kgh^{-1})
	Solvent temperature (°C)	Solvent supplement (kgh^{-1})
		Regenerate heat amount (kW)
		Cooling capacity (kW)
Cooling	Seawater temperature difference (°C)	Cooling capacity (kW)
	Seawater mass flow rate (kgh^{-1})	Pump power consumption (kW)

	Solvent temperature difference (°C)	
	Solvent mass flow rate (kgh^{-1})	
	CO_2 temperature difference (°C)	
	CO_2 mass flow rate (kgh^{-1})	
Compression	CO_2 mass flow rate (kgh^{-1})	Compressor power consumption
	Pressure difference (kPa)	(kW)
Liquification	LNG pressure (kPa)	Cold energy recovery amount
	LNG temperature difference (°C)	(kW)
	LNG mass flow rate (kgh^{-1})	

The OCCS enriches the CO_2 in the flue gas emitted from the main engine by means of an alcohol-amine solution. The waste heat from the exhaust gas and the cold energy released during the LNG regasification process are used for the solution regeneration and CO_2 liquification. After liquefaction the stored CO_2 will be sent for industrial use or permanently sequestered underground. The overall design schematic of the OCCS is shown in Fig. 4-2.

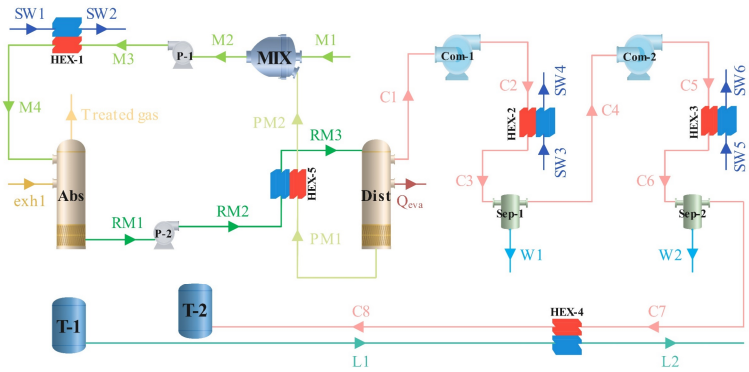

Fig. 4-2 Simulated process flow diagram of OCCS

* In this diagram, exh stands for exhaust gas; M stands for freshly prepared alcoholic amine solution; RM stands for rich liquor; PM stands for lean liquor; SW stands for seawater; W stands for water; C stands for CO_2; L stands for LNG; MIX stands for solution mixers; P stands for pump; Abs stands for absorption tower; HEX stands for heat exchangers; Com stands for compressor; Sep stands for separator; T stands for tank; Q_{eva} is the energy required to condense water vapour.

The entire simulation process consists of three subsystems:

(1) CO_2 capture subsystem: The flue gas from the main engine is cooled and part of it enters the bottom of the absorption tower, where the absorbent poor liquid comes into full contact with it by means of a spray. After exiting the absorption tower, the lean liquor absorbs the CO_2 and becomes rich liquor, then the treated flue gas is discharged into the atmosphere.

(2) Purification of CO_2 and regeneration of the solution subsystem: The cold rich liquid discharged from the absorber tower passes through the internal heat exchanger to exchange heat with the hot poor liquid discharged from the bottom of the distillation tower, which is transformed into hot rich liquid and then enters the upper part of the distillation tower for the regeneration of the solution and the purification of carbon dioxide, which is discharged from the top of the distillation tower.

(3) Liquefaction of CO_2 subsystem: In order to facilitate transportation and storage, the purified CO_2 needs to be liquefied. The CO_2 discharged from the distillation tower is compressed to 1500 kPa in two stages by a seawater heat exchanger and a compressor, then it passes through a component separator to

separate the excess impurities, and finally passes through a heat exchanger and LNG for heat exchange, using the cold energy released by LNG vaporization to liquefy the carbon dioxide.

4.2 OCCS modelling development

Aspen HYSYS V12 software is utilized to simulate the carbon capture process. The Acid Gas thermal property package and Peng-Robinson equation are applied for equilibrium calculation and kinetic reactions. The process flow process (PDF) diagram of OCCS is shown in Fig. 4-3. The main parameters are shown in Table 4-2. To simplify the calculation, the assumptions are made: (1) The adiabatic efficiency of compressor is 85%; (2) The heat loss in the whole system is neglected; (3) the extraction gas through pre-treatment process contains no high heavy hydrocarbon and saturated water.

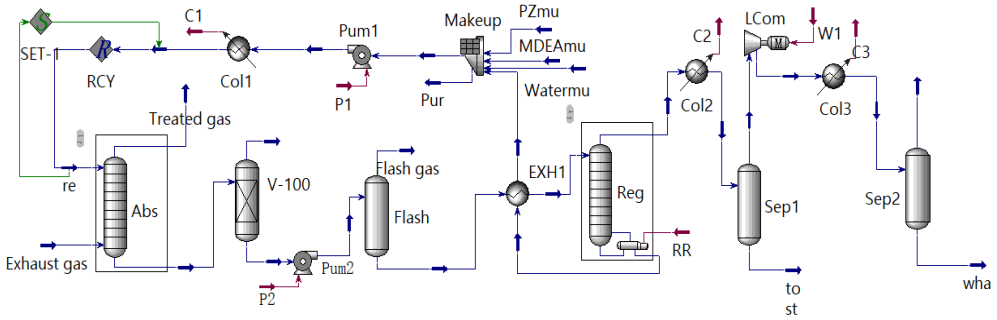

Fig. 4-3 The OCCS simulation flow diagram in HYSYS

Table 4-2 Design and operating parameters for the OCCS

Main equipment	Value
Absorber	float valve tower; trays number :10; diameter: 1.372m; tray space: 0.6096m; weir height: 0.05m; calculation method: Murphree's efficiency; lean solvent flow rate: 16000kgh^{-1}; inlet temperature: 30°C; inlet pressure: 450kPa; upper pressure: 190kPa; lower pressure: 200kPa
Stripper	float valve tower; trays number :10; diameter: 1.5m; tray space: 0.6096m; weir height: 0.05m; calculation method: Murphree's efficiency; lean solvent inlet temperature: 80°C; inlet pressure: 300kPa; upper pressure: 150kPa; lower pressure: 200kPa; reflux ratio: 10
Internal heat exchanger	shell-tube type
Pumps	lean pump: from 190 to 300kPa and isentropic efficiency of 75% rich pump: from 200 to 450kPa and isentropic efficiency of 75%
Compressor	from 150 to 1500kPa, isentropic efficiency of 75%, outlet temperature is cooled to 60°C
HEX	shell-tube type; HEX1 hot side: from 60 to 30°C and pressure drop is 0kPa; HEX2 outlet temperature 60°C and pressure drop is 0kPa
Cooler	shell-tube type; coolant: water

The compositions of the exhaust gas obtained from the main engine are presented in Table 4-3. Considering the energy balance, only part of the exhaust gas passed through the OCCS, while the rest was discharged to the environment.

Table 4-3 Composition of the exhaust gas

Component	Mass fraction (%)
Nitrogen	75.0
Oxygen	16.6
Water	4.0
Carbon dioxide	4.4

The exhaust gas from the main engine passes through the absorption column and only CO_2 is absorbed. The treated gas is vented to the air, and the solvent becomes rich solvent. The rich solvent is pumped to the stripper column for regeneration. Before the stripper column, the rich solvent recovers heat from the lean solvent, which returns from the bottom of the re-boiler. After which, the working medium is supplemented to the original composition. The lean solvent is returned to the absorption column. The CO_2 is discharged in the gaseous state from the column upper. For the convenience of storage and transportation, the separated CO_2 is liquified. Instead of using the complex multi-stage compression process, the cryogenic cold energy released by the LNG regasification process is utilized. The CO_2 storage pressure influences the density and boiling point, which would affect the energy supplied to the OCCS.

The methyldiethanolamine (MDEA) is regarded as the ideal solvent for CCS because of its high CO_2 solubility, acceptable reaction kinetics and friendly cost. After the 1980s, MDEA was widely used in CO_2 absorption process. German BASF company added different activators (such as piperazine, butylamine, imidazole or methyl imidazole, etc.) to the MDEA solvent and successfully developed activation methods for MDEA. MDEA acts as both an electrolyte and a mixed solvent system, so both chemical absorption and physical absorption occur at the same time. MDEA does not react with CO_2 directly but catalyzes the hydrolysis of CO_2. In this study, to improve reaction rate and reduce column height, the MDEA with PZ as the activator is used as the working medium for CO_2 capture. The activated solvent is with the solubility of 22 wt% MDEA and 8 wt% PZ.

The activated solution is with the highest solubility of 22 wt% MDEA and 8 wt% PZ. The equilibrium and kinetics-controlled reactions of the MEDA-PZ-CO_2-H_2O mixture have been well investigated. The stoichiometry of the MEDA with PZ as the activator is showed:

$$2H_2O \leftrightarrow^{K_1} H_3O^+ + OH^- \tag{4-1}$$

$$CO_2 + 2H_2O \leftrightarrow^{K_2} H_3O^+ + HCO_3^- \tag{4-2}$$

$$HCO_3^- + H_2O \leftrightarrow^{K_3} H_3O^+ + CO_3^{2-} \tag{4-3}$$

$$PZH^+ + H_2O \leftrightarrow^{K_4} PZ + H_3O^+ \tag{4-4}$$

$$PZ + CO_2 + H_2O \leftrightarrow^{K_5} PZCOO^- + H_3O^+ \tag{4-5}$$

$$HPZCOO^- + H_2O \leftrightarrow^{K_6} PZCOO^- + H_3O^+ \tag{4-6}$$

$$PZCOO^- + CO_2 + H_2O \leftrightarrow^{K_7} PZ(COO^-)_2 + H_2O \tag{4-7}$$

$$MEDA + H_2O \leftrightarrow^{K_8} MEDAH^+ + OH^- \tag{4-8}$$

The equilibrium constants (K_i) for reactions in MEDA were calculated from the reference state Gibbs free energies of the participating components by Eq. (15).

$$-RT \ln K_i = \Delta G_i \tag{4-9}$$

Where, R is the universal vapor constant, T is the temperature, ΔG is the Gibbs energy change for the reaction process i.

The kinetics-controlled reactions are determined by the power law equation:

$$r_q = k_q T^n \exp(-\frac{E_q}{RT}) \prod_{i=1}^{N} (x_i \gamma_i)^{\varepsilon_{iq}} \tag{4-10}$$

Where, r_q it the reaction rate for the reaction process q, k_q is the pre-exponential factor, T^n is the system temperature, x_i and γ_i are the molar fraction and the activity coefficient of the component i, and ε_{iq} is the component i stoichiometric in the reaction process q.

The carbon capture rate that can be achieved by OCCS is an important measure of OCCS capacity. However, the regenerative heat consumption is also an important indicator of the system. Therefore, the regenerative heat consumption required to capture a unit mass flow of CO_2 is called specific heat consumption denoted by ε, as follows:

$$\varepsilon = \frac{3.6 Q_{dist}}{m_{CO_2,ca}} \tag{4-11}$$

Where, Q_{dist} stands for the regeneration heat required for distillation column, measured in kW; $m_{CO_2,ca}$ stands for the mass flow rate of captured CO_2, measured in kg/h.

Furthermore, the thermodynamic performance of the whole system will be measured by the energy efficiency and exergy efficiency. The specific definitions are shown below:

$$\eta_{e_n} = \frac{W_{net}}{W_{in}} \tag{4-12}$$

Where, η_{e_n} is the total energy efficiency of OCCS; W_{net} is the net gain work of OCCS, measured in kW; W_{net} is the total input energy in the system, measured in kW.

The equation for the work of each parameter point is as follows:

$$W = mh \tag{4-13}$$

Where, m is mass flow rate corresponding to each parameter point; h is specific enthalpy. Table 4-4. shows the energy calculation formula for equipment.

Table 4-4 Energy calculation formula for equipment

Equipment	Energy payment (kW)	Energy income (kW)
HEX-1	$m_{SW1}(h_{SW2} - h_{SW1})$	$m_{M3}(h_{M3} - h_{M4})$
HEX-2	$m_{SW3}(h_{SW4} - h_{SW3})$	$m_{C2}(h_{C2} - h_{C3})$
HEX-3	$m_{SW5}(h_{SW6} - h_{SW5})$	$m_{C5}(h_{C5} - h_{C6})$
HEX-4	$m_{L1}(h_{L2} - h_{L1})$	$m_{C7}(h_{C7} - h_{C8})$
HEX-5	$m_{PM1}(h_{PM1} - h_{PM2})$	$m_{RM2}(h_{RM3} - h_{RM2})$
P-1	$m_{M2}(h_{M3} - h_{M2})$	$m_{M2}(h_{M3} - h_{M2})/95\%$
P-2	$m_{RM2}(h_{RM3} - h_{RM2})$	$m_{RM2}(h_{RM3} - h_{RM2})/95\%$
Com-1	$m_{C1}(h_{C2} - h_{C1})$	$m_{C1}(h_{C2} - h_{C1})/95\%$
Com-2	$m_{C4}(h_{C5} - h_{C4})$	$m_{C4}(h_{C5} - h_{C4})/95\%$
Dist	$m_{C1}h_{C1} + m_{PM1}h_{PM1} + Q_{eva} - m_{RM3}h_{RM3}$	$Q_{exh,in}$

*This system assumes an energy efficiency of 95% for the pump and compressor; value of Q_{eva} (energy required for water vapour condensation reflux) and $Q_{exh,in}$ (regenerative heat consumption) is given by Aspen HYSYS V12.

The following is definition of exergy efficiency:

$$\eta_{e_x} = \frac{E_{x,in}}{E_{x,pay}} \tag{4-14}$$

Where, η_{e_x} is the total exergy efficiency of OCCS; $E_{x,in}$ is exergy of income, measured in kW; $E_{x,pay}$ is exergy of payment, measured in kW.

Furthermore, this paper adds a chemical exergy part to the whole exergy analysis which make it more rational and precise. Exergy (E_x) is made up of physical exergy ($E_{x,ph}$) and chemical exergy ($E_{x,ch}$). As follows:

$$E_x = E_{x,ph} + E_{x,ch} \tag{4-15}$$

The physical exergy of liquid each parameter point in the system is defined as:

$$E_{x,ph} = m \cdot \psi \tag{4-16}$$

Where, m is mass flow rate corresponding to each parameter point; ψ is specific physical exergy, which is defined as:

$$\psi = (h - h_0) - T_0 \cdot (s - s_0) \tag{4-17}$$

Where, h and s respectively represent the specific enthalpy and specific entropy of each flow unit in the system under given actual working conditions; h_0 and s_0 respectively represent the specific enthalpy and specific entropy of each flow unit in the system under ambient conditions; T_0 is the reference state temperature, T_0=298K.

The chemical exergy of liquid each parameter point in the system is defined as:

$$E_{x,ch} = n \cdot \varphi \tag{4-18}$$

Where, n is the mole flow rate corresponding to each parameter point; φ is specific chemical exergy, which is defined as:

$$\varphi = \sum_i x_i \varepsilon_{ch_i} + RT_0 \sum_i x_i \ln x_i \tag{4-19}$$

Where, x_i is mole fraction of component i; ε_{ch_i} is standard chemical exergy of component i; R is the universal gas constant.

Heat exergy of distillation column is defined as:

$$E_{x,Q} = Q \cdot (1 - \frac{T_0}{T}) \tag{4-20}$$

Where, Q is the energy of the heat flow absorbed or released during the reaction in the distillation column; T_0 is the reference state temperature, T_0=298K, T represents the temperature under ambient conditions.

Table 4-5. shows exergy calculation formula for equipment.

Table 4-5 Exergy calculation formula for equipment

Equipment	Exergy payment (kW)	Exergy income (kW)
HEX-1	$m_{M2}(\psi_{M2} - \psi_{M3})$	$m_{SW1}(\psi_{SW2} - \psi_{SW1})$
HEX-2	$m_{C2}(\psi_{C2} - \psi_{C3})$	$m_{SW3}(\psi_{SW4} - \psi_{SW3})$
HEX-3	$m_{C5}(\psi_{C5} - \psi_{C6})$	$m_{SW5}(\psi_{SW6} - \psi_{SW5})$
HEX-4	$m_{L1}(\psi_{L1} - \psi_{L2})$	$m_{C7}(\psi_{C8} - \psi_{C7})$
HEX-5	$m_{PM1}(\psi_{PM1} - \psi_{PM2})$	$m_{RM2}(\psi_{RM3} - \psi_{RM2})$
P-1	$m_{M2}(h_{M3} - h_{M2})$/95%	$m_{M1}(\psi_{M2} - \psi_{M1})$
P-2	$m_{RM2}(h_{RM3} - h_{RM2})$/95%	$m_{RM1}(\psi_{RM2} - \psi_{RM1})$

Com-1	$m_{C1}(h_{C2}-h_{C1})/95\%$	$m_{C1}(\psi_{C2}-\psi_{C1})$
Com-2	$m_{C4}(h_{C5}-h_{C4})/95\%$	$m_{C3}(\psi_{C4}-\psi_{C3})$
Dist	$E_{x,Q_{exh,in}}-E_{x,Q_{eva}}$	$(m_{C1}\cdot\psi_{C1}+m_{PM1}\cdot\psi_{PM1}-m_{RM1}\cdot\psi_{RM1})$ $+(n_{C1}\cdot\varphi_{C1}+n_{PM1}\cdot\varphi_{PM1}-n_{RM1}\cdot\varphi_{RM1})$
Abs	$m_{exh1}\cdot\psi_{exh1}+n_{exh1}\cdot\varphi_{exh4}$ $+m_{M4}\cdot\psi_{M4}+n_{M4}\cdot\varphi_{M4}$	$m_{Exh2}(\psi_{Exh2}-\psi_{Exh3})$

The thermodynamic analysis of the system alone is unable to fully verify its feasibility, Further consideration needs to be given to economic factors such as the initial investment cost and operation and maintenance costs of the equipment in the system. Therefore, the economic analysis contributes to understand the feasibility of the proposed onboard carbon capture system. Based on the thermodynamic analysis of the system, an economic evaluation was carried out and listed the initial investment cost functions of the main components of the system.

The total investment cost rate of the system includes the initial investment cost rate $\dot{Z}_{CI,k}$ and the operation and maintenance cost rate $\dot{Z}_{OM,k}$ for each component.

$$\dot{C}_{total}=\sum_k(\dot{Z}_{CI}+\dot{Z}_{OM})_k \tag{4-21}$$

Where, the initial investment cost rate $\dot{Z}_{CI,k}$ and the operation and maintenance cost rate $\dot{Z}_{OM,k}$ of the component k can be defined as:

$$\dot{Z}_{CI,k}+\dot{Z}_{OM,k}=\frac{Z_k\cdot\phi}{N\cdot 3600}\cdot CRF \tag{4-22}$$

Where, Z_k is the initial investment cost of component k, ϕ is the maintenance factor for system operation, taken as 1.06, N is the annual operating time of the system, taken as 7300 hours here, and CRF is the capital recovery factor, which can be defined as:

$$CRF=\frac{i(1+i)^{\tau}}{(1+i)^{\tau}-1} \tag{4-23}$$

Where, τ denotes the system life cycle, taken 20 years, and i denotes the annual interest rate, taken as 0.14.

The investment cost functions of system components are given in Table 4-6.

Table 4-6 Investment cost functions of system components

Component	Investment cost function
Heat exchanger	$Z_{HEX}=130\cdot(\frac{A_{HEX}}{0.093})^{0.78}$
Compressor	$Z_{Com}=\frac{71.1\cdot m}{0.9-\eta_{is}}\cdot r_p\cdot\ln(r_p)$
Pump	$Z_{Pump}=800\cdot(\frac{W_{Pump}}{10})^{0.26}\cdot(\frac{1-\eta_{Pump}}{\eta_{Pump}})^{0.5}$
Absorption tower & Distillation column	$Z_{Dist}=Z_{vessel}+Z_{tray}$ $Z_{vessel}=1780\cdot l^{0.87}\cdot d^{1.23}[2.86+1.694\cdot F_M(10.01-7.408\cdot\ln(P)+1.395\cdot\ln^2 P)]$ $Z_{tary}=(193.04+22.72\cdot d+60.38\cdot d^2)\cdot F_{BM}\cdot N_{act}\cdot f_q$
Separator	$Z_{Sep}=309.14\cdot(A_{Sep})^{0.85}$

In the table above, r_p is the pressure radio; η_{is} is the isentropic efficiency; l is the length or height of the

column; d is the diameter of the column; F_M is the material factor; F_{BM} is the Bare-Module factor; N_{act} is the actual number trays and f_q is the quantity factor. In this system, the material of column and tray is stainless steel, hence the values of F_M and F_{BM} are taken as 4.0 and 2.0 respectively. If the actual number of column trays is greater than 20, then the value of f_q is taken as 1.0.

4.3 Results and discussion

Fig. 4-4 shows the effect of lean liquor temperature (T_{sol}) at the inlet of the absorber tower on CO_2 capture (m_{CO_2}) and specific heat consumption (ε) under the condition of exhaust gas mass flow rate of 22,000 kg/h and lean liquor mass flow rate of 18000 kg/h at the inlet. As the temperature of the lean liquor increases from 20°C to 60°C, the amount of CO_2 captured gradually decreases, this is because as the temperature increases, the solubility of CO_2 in the lean liquor decreases, which leads to a reduction in the heat of regeneration required and a decrease in specific heat consumption from 5.34 GJ/tCO_2 to 5.24 GJ/tCO_2. In this paper, the greatest reduction in specific heat consumption, but the least reduction in CO_2 capture, occurs at 35°C to 40°C, so a background working condition of 40°C is selected.

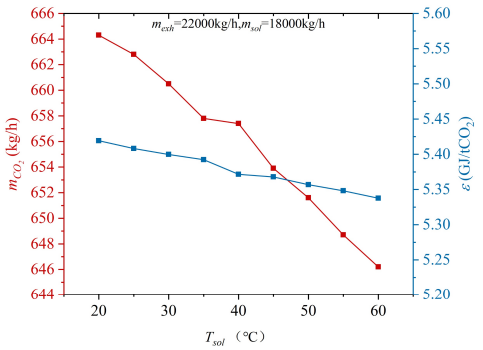

Fig. 4-4 Effect of lean liquor temperature on CO_2 capture

Fig. 4-5 shows the effect of exhaust gas mass flow rate (m_{exh}) and lean liquor mass flow rate (m_{sol}) at the inlet of the absorption tower on the amount of CO_2 captured (m_{CO2}). In order to visualise the carbon capture capacity of the OCCS system, the lower limit value of CO_2 emission for the second and third stages of the EEDI (113.7 kg/h and 613.8 kg/h) are indicated in the graph. It is easy to see that when the two masses are controlled at 40°C, the CO_2 capture increases significantly with the increase in mass flow rate of exhaust gas and lean liquor, but the rate of increase slows down after a certain point. In summary, OCCS systems can meet EEDI Stage III requirements when the solution mass flow rate is greater than 13000 kg/h. Optimum operating condition can be positioned at 20000 kg/h.

Fig. 4-6 and Fig. 4-7 show the regenerative heat consumption ($Q_{exh,in}$) and specific heat consumption (ε) of OCCS, respectively. It can be observed that as the mass flow rate of the exhaust gas increases, the amount of CO_2 absorbed increases, but the heat of regeneration required by the distillation column also increases. At the same time, the heat of regeneration increases with increasing mass flow rate of the solution when the mass flow rate of the exhaust gas is constant. As for the dramatic reduction in specific heat consumption, although both regeneration heat consumption and CO_2 capture increase as the exhaust gas mass flow rate increases, the rate of increase in regeneration heat consumption is much less than the rate of increase in CO_2 volume.

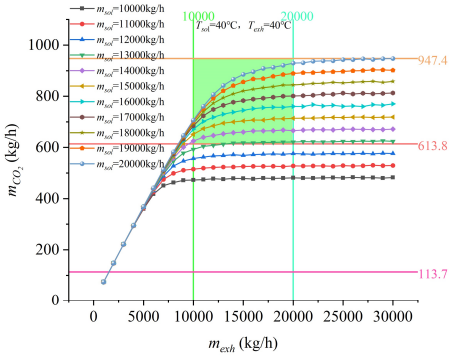

Fig. 4-5 Effect of mass flow rate of exhaust gas and lean liquor on the amount of CO_2 captured

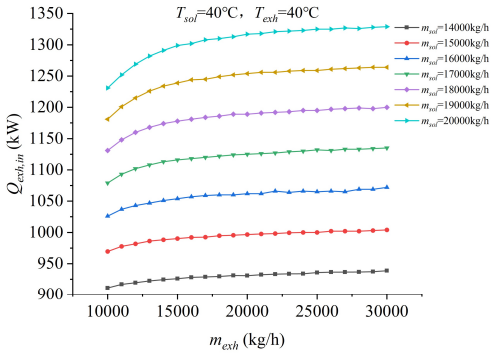

Fig. 4-6 Regenerative heat consumption

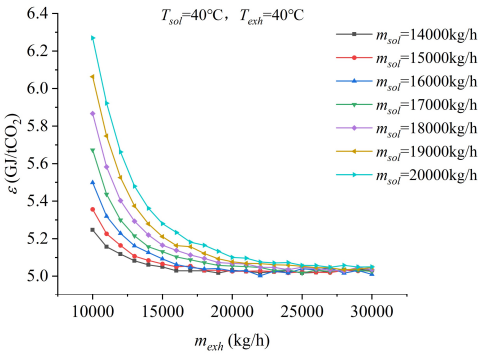

Fig. 4-7 Specific heat consumption

Fig. 4-8 shows the energy efficiency (η_{en}) and exergy efficiency (η_{ex}) of the entire system respectively. The energy efficiency and exergy efficiency of the system increases with increasing mass flow rate of lean liquor at the optimum operating parameters of the exhaust gas mass flow rate (m_{exh}=20000 kg/h). It is clear that the energy efficiency of the system increases slowly as the mass flow rate of the lean liquor increases. As for exergy efficiency, it is stable between 44.70% and 54.66%. The maximum value occurs at the solution of 16000 kg/h. In summary, the optimum operating parameters for the working mass at

optimum operating conditions are m_{exh}=20000 kg/h, m_{sol}=16000 kg/h. The amount of CO_2 captured at this point is 760.4 kg/h, which is well above EEDI Stage 3 requirements.

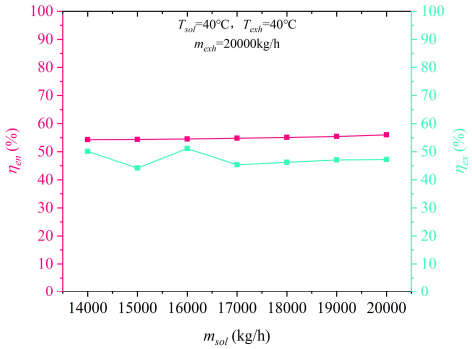

Fig. 4-8 Energy efficiency and exergy

Fig. 4-9 shows percentage of exergy income of main components in the system under the optimum operating condition. It is clear that the absorption and distillation towers account for the largest share of exergy income, which is due to their internal chemical reactions, chemical exergy is generally an order of magnitude larger than physical exergy.

According to the formula, the initial investment cost of the main equipment in the system is shown in Table 4-7. The total initial cost is 1.38 million US $.

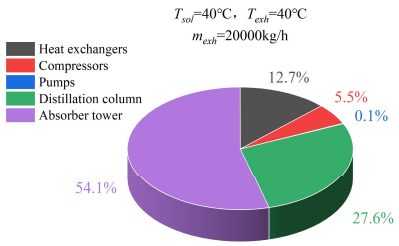

Fig. 4-9 Account for exergy income of main equipment

Table 4-7 The initial investment cost of the main equipment

Component	Initial investment cost (US $)
Heat exchangers	121741.25
Compressors	731.78
Pump	442.02
Distillation column	293458.28
Absorption tower	959190.03
Separator	1982.61

The CO_2 captured is generally used for industrial purposes and the current price of liquid carbon dioxide is US$17.3/t, which is expressed as *LCP*. So, the annual revenue (AR) of the system can be expressed as:

$$AR = \frac{7300 \cdot m_{CO_2} \cdot LCP}{1000} \tag{4-24}$$

Therefore, the payback period (PBP) of the system is defined as:

$$PBP = \frac{Z_{k,total} \cdot \phi}{ATI} \tag{4-25}$$

Based on the above formula, the annual revenue under the operation of the system is US$96,030.92 and the various costs are US$137,545.96. For this Kamsarmax model, it would take approximately 14.34 years to recover its investment cost.

4.4 Summary

In this chapter, a shipboard carbon capture system for LNG-fuelled vessels based on the integrated use of cold and heat energy is designed, guided by the EEDI Stage 3 requirements. The waste heat from exhaust gas as a source for the solution regeneration is harvested. Meanwhile, the CO_2 is liquified with the cold energy released by LNG vaporisation. A Kamsarmax vessel is taken as an example and the plasticity of the system is analysed from three perspectives: energy, exergy and economic via Aspen HYSYS. The CCS optimum operating parameters are m_{exh}=20000 kg/h, m_{sol}=16000 kg/h. The amount of CO_2 captured at this point is 760.4 kg/h, which is well above EEDI Stage 3 requirements. The total initial cost of CCS is 1.38 million US $. Considering the captured CO_2 profits, the CCS would take approximately 14.34 years to recover its investment cost. The results show that there is still space for optimisation in terms of energy use. The next stage will be the thermodynamic optimisation, environmental impact analysis and economic analysis of the OCCS system.

5. Onboard Organic Rankine Cycle combined with Carbon Capture and Storage system

Based on the results in the last chapter, it is clearly demonstrated that the LNG cold energy is over sufficient for CO_2 liquification under the context of meeting the EEDI requirement of phase 3. That is, there is still a large mount of LNG cold energy is wasted onboard. Therefore, to further use the LNG cold energy, the ORC-CCS system is proposed and investigated. The ORC could convert the waste heat and LNG cold energy into power, which would supply the energy required by the power facilities, such as compressor and pump. Thus, in this chapter, we will to find out whether the power supply by the ORC would balance the additional power required by the OCCS, namely, a zero-energy increase OCCS.

5.1 ORC-CCS design

The energy flow and CO_2 path of the LNG-fuelled ship with ORC-CCS is demonstrated in Fig. 5-1. The CCS technologies include pre-combustion carbon capture, oxy-fuel combustion carbon capture, absorption technique, and cryogenic liquification. Considering the onboard limitation, the absorption technique and cryogenic liquification would be promising selections for CCS.

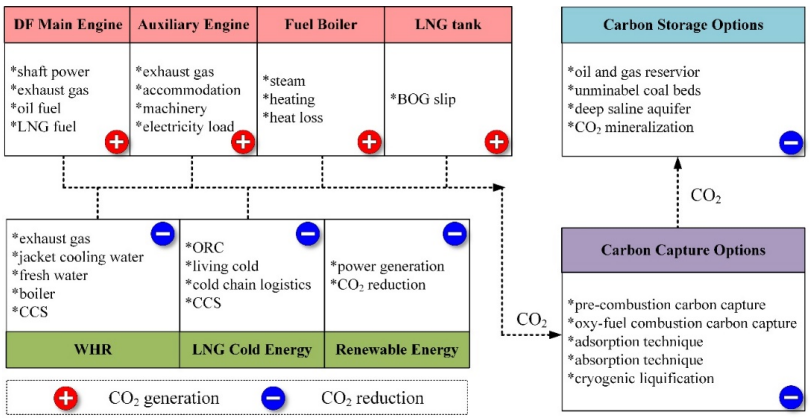

Fig. 5-1 The energy flow and CO_2 path of the LNG-fuelled ship with onboard ORC-CCS

A zero EI-OCCS for an 80000 DWT LNG-fuelled bulk carrier is proposed by integrating ORC and onboard carbon capture unit. For the ORC, the LNG cold energy and jacket cooling water are used as the cold source and the heat source, respectively. For the carbon capture unit, the chemical absorption method is adopted for CO_2 capture from the flue gas. Noticeable, the exhaust gas firstly provides thermal energy for CO_2 desorption before entering the absorber. Afterwards, the concentrated CO_2 is liquified with the low-grade LNG cold energy. The system makes full use of the ship's waste heat and cold energy without the supplement electricity.

Fig. 5-2 is a simplified diagram of the proposed system installed in the reference ship. The proposed process consists of three parts: ORC process, CO_2 capture process and CO_2 liquefaction process.

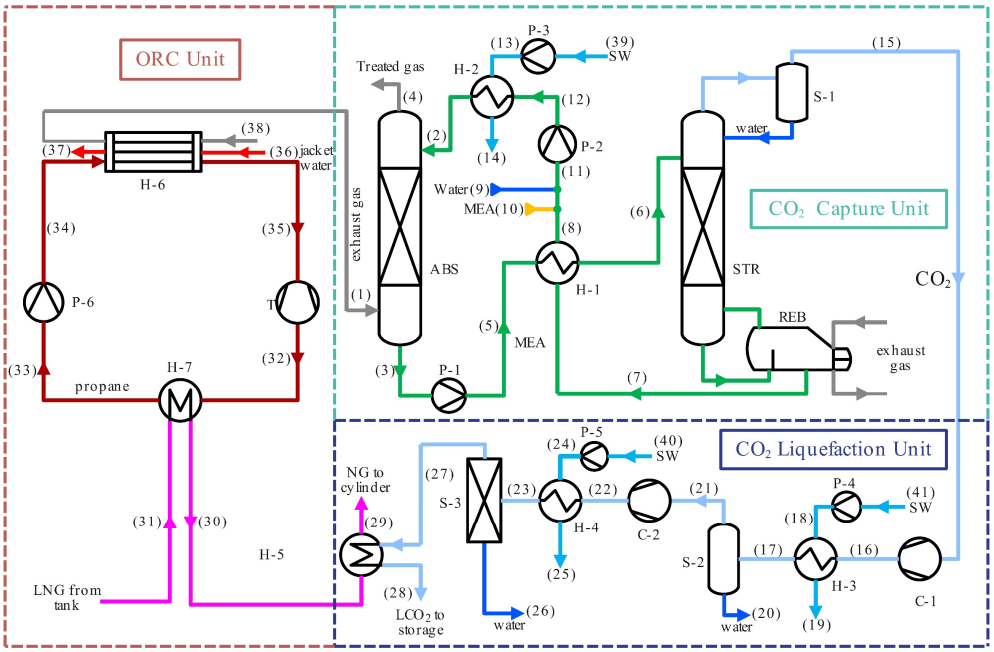

Fig. 5-2 Simplified scheme of zero EI-OCCS system.

5.1.1 ORC process

In the ORC process, LNG is used as the cooling source and stored in the compartment at a temperature of approximately -162 °C. The pressurized LNG is discharged from the compartment and supplied to the condenser (H-7) at a pressure of 600kPa. The propane is selected as the ORC working medium, which absorbs the cold energy released by the LNG gasification at atmospheric pressure and condenses to a saturated state. To maximize the power generation of the ORC, the cold energy from the phase change section is fully utilized, raising the LNG temperature to -75 °C. However, at this point, not all the cold energy has been used up, which does not meet the temperature requirement for NG entering the main engine combustion. Therefore, the excess cold energy is used to liquefy CO_2, while the temperature of NG is raised to 35 °C, and then transported to the main engine for power generation. Afterwards, the saturated propane is pressurized by the working pump (P-6) and supplied to the evaporator (H-6), where the pressure is set to 2 MPa to obtain sufficient output power. The exhaust gas, which has provided heat from the reboiler, passes through the evaporator and exchanges heat with propane, reducing the temperature from 120 °C to 50 °C, and then enters the absorber for CO_2 capture. Meanwhile, the jacket cooling water also decreases from 96 °C to 80 °C, and then returns to the cooling loop to prevent the main engine from overheating. However, the minimum temperature of the jacket cooling water should not be lower than 70 °C, otherwise the fuel in the main engine will become too cold, affecting normal operation. At the same time, the propane vapor that is heated in the propane evaporator enters the turbine (T) to generate power, which provides electricity to satisfy the electrical demand of all equipment in the system.

5.1.2 CO_2 capture process

During the CO_2 absorption and desorption process, the partially cooled exhaust gas enters the absorber (ABS) at a temperature of 50 °C and reacts with the MEA lean solution. The CO_2 in the exhaust gas is absorbed by the MEA lean solution in the column. As a result, the treated gas (which contains almost

no CO_2) is directly discharged into the atmosphere, while the MEA-rich solution discharged from the bottom of the absorber is transported to the stripper (STR) by pump (P-1). The MEA-rich solution is then heated by hot MEA-lean solution coming out from the bottom of the stripper. The recuperator (H-1) makes the MEA-rich solution temperature to around 80 °C to reduce the load of the reboiler. Subsequently, the cooled MEA lean solution is replenished with MEA and water to compensate for the solution loss. The cooled MEA lean solution then passes through the seawater heat exchanger (H-2) to decrease its temperature to around 50 °C, which is suitable for absorption. The cooled MEA-lean solution re-enters the absorber to react with the exhaust gas. Then, the preheated MEA-rich solution enters the stripper to desorb CO_2. To integrate ship waste heat, the exhaust gas from the main engine is fed into the reboiler to provide heat for CO_2 regeneration. In the reboiler, the temperature of the exhaust gas drops to 120 °C while the MEA solution absorbs heat to desorb CO_2, carrying away a large amount of water vapor and a small amount of MEA solute. Therefore, to obtain pure CO_2, the mixed gas leaving the tower's upper part needs to be separated using a phase separator (S-1) to remove the water, which is then entirely refluxed to the stripper. The extracted CO_2 from the separator is then subjected to compression and liquefaction.

5.2.3. CO_2 liquefaction process

During the CO_2 compression and liquefaction process, a two-stage compression method with inter-stage cooling is employed to prevent high exhaust temperature that may damage the equipment. Firstly, CO_2 is pressurized to 500 kPa by a low-pressure compressor (C-1), and then its temperature is reduced to 40 °C by a seawater heat exchanger (H-3). The CO_2 then enters a separator (S-2) to remove excess water. Afterwards, it is compressed to 1500 kPa by a high-pressure compressor (C-2). The cooling and separation steps are repeated until the CO_2 purity reaches 100%. Next, the temperature of the CO_2 is reduced to -30 °C in a condenser (H-5) utilizing excess cold energy from natural gas. As shown by the CO_2 phase diagram, the CO_2 is in a liquid state at this temperature and pressure. Finally, the liquid CO_2 is stored into tanks for further process.

5.2 ORC-CCS modelling development

5.2.1. Simulation basis

Aspen HYSYS V12 is utilized to simulate the zero EI-OCCS process. The Acid Gas thermal property package and Peng-Robinson equation are applied for equilibrium calculation and kinetic reactions. The main parameters are shown in Table .The assumptions of the proposed system are made: (1) steady-state and adiabatic condition for all equipment. (no heat exchange with the environment). (2) The exhaust gas composition on a mass basis is of 73.1% nitrogen, 11.2% oxygen, 5% water and 10.7% carbon dioxide. (3) The LNG reference composition is assumed as 100% methane. (4) In the two-stage compression process, the cooling temperature of desorbed CO_2 is 40 ℃. (5) The maximum amount of regeneration heat that the main engine can provide is 3106.3 kW.

Table 5-1 Parameters assumed for system.

	Parameter	**Value**
ORC process	Jacket cooling water inlet temperature	96 ℃
	Propane liquid quality at the propane pump inlet	1
	Propane liquid quality at the vaporizer outlet	0
	Turbine isentropic efficiency	85%
CO_2 capture process	MEA mass concentration	30%
	MEA and exhaust gas inlet temperature	50 ℃

CO_2 compression and liquefaction process	Absorber and stripper packing type	Mellapak 500Y
	Absorber and stripper stage number	10
	Desorbed gas temperature after each heat exchanger	40 ℃
	Seawater inlet temperature	30 ℃
	Seawater inlet pressure	200kPa

5.2.2. Modeling

The work produced by the turbine is defined as:

$$W_T = \dot{m}_T (h_{T,in} - h_{T,out}) \tag{5-1}$$

Where, $\dot{m}_T$ is the mass flow rate of the propane through the turbine; $h_{T,out}$ and $h_{T,out}$ are the specific enthalpies of propane at the inlet and outlet of the turbine.

The electricity demand of the zero-EI OCCS is:

$$W_{demand} = \sum W_P + \sum W_C \tag{5-2}$$

Where, W_P and W_C are the work consumed bu the pumps and compressors.

To define the amount of captured CO_2 , f_{CO2} is used to present the carbon capture rate of the system:

$$f_{CO_2} = \frac{\dot{m}_{CO_2,cap}}{\dot{m}_{CO_2,exh}} \tag{5-3}$$

Where, the $\dot{m}_{CO2\ ,cap}$ and $\dot{m}_{CO2\ ,exh}$ are the mass of captured CO_2 and exhaust gas contained CO_2 , respectively.

The specific reboiler duty can be defined as:

$$\varepsilon = \frac{Q_{reg}}{\dot{m}_{CO_2,cap}} \tag{5-4}$$

Where, Q_{reg} is the regenerative heat consumed by the stripper.

To determine the profits of the liquefied CO_2 , the heat duty of H-3 and H-4 can be regarded as the produced energy because the seawater is free, and the electrical demand of seawater pumps can be supplied by the ORC. Therefore, the energy efficiency of the zero-EI OCCS is defined as:

$$\eta_{en,sys} = \frac{W_T + Q_{LNG,CO_2} + Q_{H-3} + Q_{H-4}}{Q_{reg} + Q_{jcw} + Q_{exh} + Q_{LNG,tot} + W_{demand}} \tag{5-5}$$

Where, $Q_{LNG,CO2}$ is the cold energy of LNG liquefied CO_2 in H-5; Q_{reg} is the heat supplied by exhaust gas to the reboiler; Q_{jcw} is the heat of the jacket cooling water in H-6; Q_{exh} is the heat of the exhaust gas in H-6; $Q_{LNG,tot}$ is the cold energy of LNG in H-7 that is fully utilized before it enters the main engine for combustion.

Exergy analysis defines the max useful work obtained from the system by calculating the irreversibility in the process. Since the process has little variation in height and velocity, the potential exergy and kinetic exergy can be neglected. Thus, the total exergy is presented as:

$$\dot{E}_x = \dot{m}(e_{ph} + e_{ch}) \tag{5-6}$$

Where, e_{ph} is the physical exergy; e_{ch} is the chemical exergy of the fluid [84].

During chemical reaction and heat or mass transfer, the exergy destruction occurs due to increased entropy. The exergy destruction of the equipment in system are given by:

$$\dot{E}_D = \dot{E}_{pay} - \dot{E}_{income} \tag{5-7}$$

The exergy destruction ratio of the equipment is expressed as:

$$\varphi_i = \frac{\dot{E}_{D,i}}{\dot{E}_{D,sys}} \tag{5-8}$$

Where, $\dot{E}_{D,i}$ is the i^{th} component exergy destruction and $\dot{E}_{D,sys}$ is the system exergy destruction.

Based on above, the system exergy efficiency is defined as:

$$\eta_{ex,sys} = \frac{\dot{E}_{LCO_2} + W_T + \dot{E}_{jcw,out} + \dot{E}_{NG,out} + \dot{E}_{tg}}{W_{demand} + \dot{E}_{mu} + \dot{E}_{exh,in} + \dot{E}_{jcw,in} + \dot{E}_{LNG,in}} \tag{5-9}$$

Where, $\dot{E}_{mu}$ is the exergy flow rate of replenished water and MEA; $\dot{E}_{jcw,in}$ and $\dot{E}_{jcw,out}$ are the exergy flow rate of inlet and outlet jacket cooling water; $\dot{E}_{LNG,in}$ and $\dot{E}_{NG,out}$ are the exergy flow rate of inlet and outlet natural gas; $\dot{E}_{tg}$ is the exergy flow rate of treated gas; $\dot{E}_{exh,in}$ is the exergy flow rate of inlet exhaust gas in ORC process; $\dot{E}_{LCO2}$ is the exergy flow rate of the liquefied CO_2.

For large-scale systems, economic analysis is essential in the process of designing and implementing solutions, because some designs may not be practical and economic benefits may not meet expectations. Therefore, a comprehensive economic analysis of the system should be carried out during simulation to minimize unnecessary losses. To analyse the economic benefits of the system, the calculation of costs should start with the total cost, which consists of total investment costs and total operating costs. Using some evaluation indicators, the economic efficiency of the system can be measured.

Total investment cost (TIC)

Total investment costs include the cost of purchasing equipment and the cost of initial materials. This paper adopts a modular cost calculation method to calculate the equipment cost of the system. The calculation method is as follows:

$$\lg C_{PE} = K_1 + K_2 \lg Y + K_3 (\lg Y)^2 \tag{5-10}$$

Where, C_{PE} is the purchase equipment cost; Y is the capacity or size parameter of the equipment.

After calculating C_{PE}, the bare module cost can be calculated as follow:

$$C_{BM} = C_{PE} \cdot f_{BM} \tag{5-11}$$

Where, C_{BM} is the bare module cost; f_{BM} is the bare module factor.

$$f_{BM} = B_1 + B_2 \cdot f_M \cdot f_P \tag{5-12}$$

Where, f_M is the factor of materials; f_P is the factor of pressure.

$$\lg f_P = C_1 + C_2 \lg P + C_3 (\lg P)^2 \tag{5-13}$$

Where, P is the pressure of the equipment in bar.

Furthermore, to consider the inflation effect on equipment costs, the Chemical Engineering Plant Cost Index (CEPCI) is adopted. The purchase cost of each equipment in the year 2020 can be estimated by:

$$C_{BM,2020} = C_{BM,2001} \cdot \frac{CEPCI_{2020}}{CEPCI_{2001}} \tag{5-14}$$

Where, $CEPCI_{2020}$ is 596.2 and the $CEPCI_{2001}$ is 394.3.

After calculating all needed data, the total capital investment can be calculated by:

$$TIC = \sum C_{BM} + C_f \tag{5-15}$$

Where, C_f is the initial cost of all working fluid in system.

Total operating cost

The total operating cost (TOC) consists of the fixed operating cost (FOC) and the variable operating cost (VOC). The fixed operating cost includes the costs of maintenance, labour, local taxes and insurance, administration, laboratory, supervision, etc. For ORC, it was assumed as 1.65% of TCI, while for the capture and compression units, it was considered as 3% of the TCI. The variable operating cost is the

annual sum of utility and make-up stream costs. The total electricity consumption is equal to the electricity produced in the ORC minus the sum of the electricity consumed by compressors, pumps and blower.

$$TOC = FOC + VOC \tag{5-16}$$

Economic indices

The total annual cost (TAC) is the bases for economic analysis and can be given by:

$$TAC = TIC_{anu} + TOC \tag{5-17}$$

$$TIC_{anu} = TIC \cdot CRF \tag{5-18}$$

$$CRF = \frac{i(i+1)^n}{(i+1)^n - 1} \tag{5-19}$$

Where, n is plant lifetime (25 years) and i is the interest rate (10%).

One of the most important indices in the analysis of the CCS is the CO_2 capture cost (CCC), and with this index, the data obtained from different works can be compared with each other. This index can be expressed as the total annual cost divided by the total mass flow rate of captured CO_2:

$$CCC = \frac{TAC}{m_{CO_2,cap}} \tag{5-20}$$

5.3 Results and discussion

Fig 5-3 shows the variation in CO_2 capture amount of the system with changes in the mass flow rate of exhaust gas and MEA solution. When the mass flow rate of exhaust gas increases, the CO_2 capture amount also increases. It is worth noting that when the mass flow rate of solution are 13000 kg/h and 15000 kg/h, the CO_2 capture amount does not vary much with the exhaust gas flow rate. This is because the amount of CO_2 that the solution can absorb is limited, and under these two operating conditions, the CO_2 load of the solution at a fixed flow rate has already approached the limit. When the solution flow rate is increased, the CO_2 capture amount increases significantly and gradually levels off as the solution approaches saturation. When the solution flow rate is 21000 kg/h and the exhaust gas flow rate is 20000 kg/h, the maximum amount of captured CO_2 is 1686 kg/h.

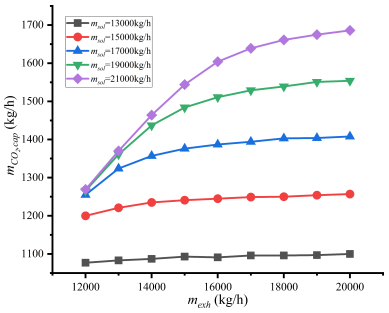

Fig. 5-3 Effect of various m_{exh} and m_{sol} on the mass flow rate of captured CO_2.

Fi 5-4 presents the relationship between solution flow rate and specific reboiler duty, CO_2 capture rate, and the system energy efficiency. As illustrated in the figure, an increase in solution flow rate leads to a continuous rise in specific heat consumption, increasing from 4.62GJ/tonCO_2 to 4.71GJ/tonCO_2 , and the trend accelerates gradually. This is due to the significant changes in regeneration heat with the variation of solution flow rate. Additionally, Fig shows that the CO_2 capture amount experiences a slower increase as the solution flow rate grows, which results in the accelerated increase of specific reboiler duty. Furthermore, since the solution's CO_2 load is limited, the CO_2 capture rate gradually

increases from 51.31% to 78.64%. Increasing solution flow rate will greatly increase the system's heat load. The energy efficiency of the system decreases from 11.51% to 11.36%. As the CO_2 capture rate increases, the system energy efficiency and specific reboiler duty both trend towards unfavorable conditions.

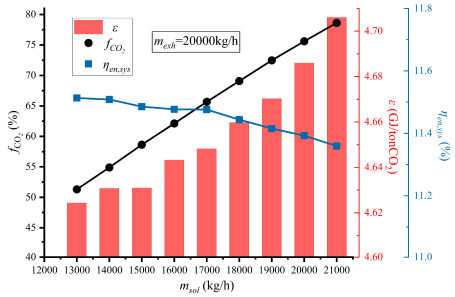

Fig. 5-4 Effect of various m_{sol} on: CO_2 capture rate, te specific reboiler duty and the system energy efficiency.

It is evident from Fig 5-5 that at any solution flow rate, the electrical energy output by the turbine can exceed the electricity demand of the system, reaching a maximum value of 123.7 kW at a solution flow rate of 21000 kg/h. At the same time, the regeneration heat also reaches its maximum value of 2204 kW. Therefore, under these boundary conditions, it is possible to achieve zero energy increment of the system. At the highest system load, the CO_2 capture rate of 78.64% is an acceptable result. At the same time, the system exergy efficiency increases from 19.59% to 28.03% as the solution flow rate increases. This is because when the exhaust gas flow rate is fixed, the increase in solution flow rate leads to an increase in CO_2 capture amount and a decrease in the flow rate of the treated gas. In addition, the output power of the turbine also increases, leading to an increase in system exergy efficiency.

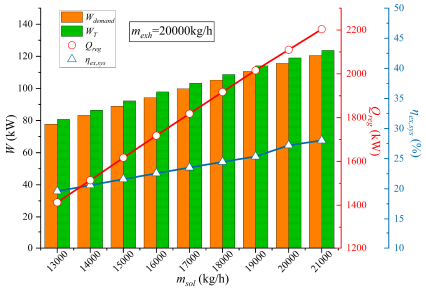

Fig. 5-5 Effect of various m_{sol} on W_{demand}, W_T, the system exergy efficiency and the reboiler duty.

Fig demonstrates the exergy destruction ratio of each equipment. The exergy destruction proportion of absorber and stripper is the largest, accounting for 39.9% and 43.3% respectively, due to the chemical reactions inside the column. Besides, because LNG and CO_2 both undergo phase changes in H-7 and the working temperature difference is large, the exergy destruction ratio of H-7 accounts for 9.4%. All the pumps have very little destructions, which is due to the small variation in temperature difference.

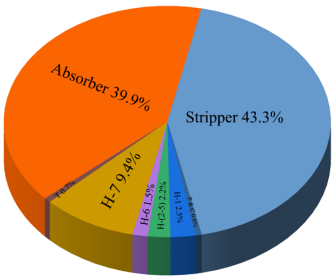

Fig. 5-6 The exergy destruction of main equipment.

Fig. 5-7 illustrates main equipment capital investment percentage in EI-OCCS system. Noticeably, the equipment capital investment is mainly from the heat exchanger, which accounts for 48.5%. This is because this system has many heat exchangers and the temperature difference in heat transfer is so large, which means high cost. Turbine capital investment is the second highest in system, with 20.7%.

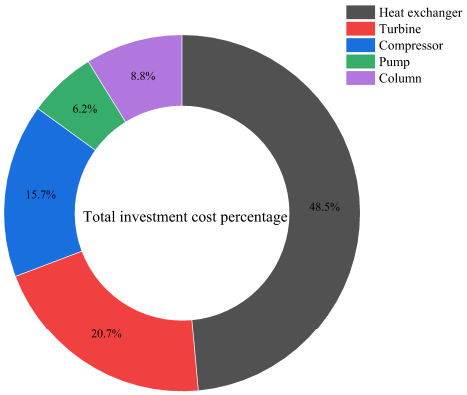

Fig. 5-7 The total investment cost percentage of main equipment

Fig 5-8 presents the relationship between the CO_2 capture cost and the exhaust gas flow rate. As the flue gas flow rate increases, it can be seen that the CO_2 capture cost decreases significantly. This is because under the condition that the solution flow rate is fixed, an increase in flue gas flow rate will increase the amount of captured CO_2, but the trend gradually slows down as the solution becomes saturated.

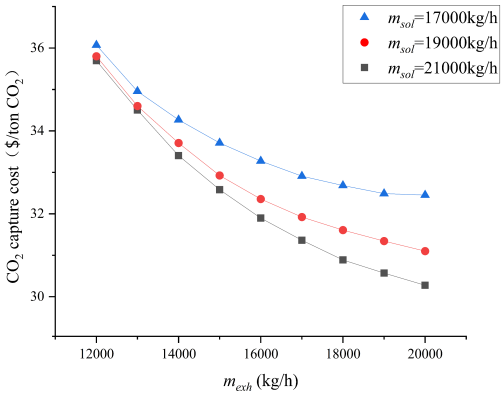

Fig. 5-8 The economic indices with the variation of m_{exh}

5.4 Summary

In this section, a zero energy increment OCCS for LNG-fueled bulk carrier with an ORC that integrates waste heat and cold energy for electrical power supplement. The system is analyzed in the study from energy, exergy and economic standpoint. The main conclusion drawn from the study are as follows: under the designed working conditions, the ORC system can generate enough electricity to fully meet the system's electricity demand. The maximum power generated by the ORC is 123.7 kW and CO_2 capture rate also reaches 78.64%. Meanwhile, the system exergy efficiency increases from 19.59% to 28.03%. Increasing the exhaust gas flow rate will increase the amount of captured CO_2 , but there is an upper limit to the capture amount. When the solution flow rate is 21000 kg/h and the exhaust gas flow rate is 20000 kg/h, the maximum amount of captured CO_2 is 1686 kg/h. The system energy efficiency increases with the increase of exhaust gas flow rate and decreases with the increase of solution flow rate. As the CO_2 capture amount changes slowly and the regeneration heat changes significantly with the solution, the specific reboiler duty also increases from 4.62GJ/tonCO_2 to 4.71GJ/tonCO_2. The equipment capital investment is mainly from the heat exchanger, which accounts for 48.5%.

6. A Pilot-Scale CCS Experimental Setup Design

6.1 Pilot-Scale CCS capacity description

For further investigate the performance of the carbon capture system, a pilot-scale experimental setup is designed. The designed CCS aims at capturing10 kg/h CO_2. For the engineering application, the commonly used 30% MEA solution is used for CO_2 enrichment. Considering the safety and environment requirement on campus, the liquid nitrogen (LN2) is used to simulate LNG to provide the cryogenic temperature for CO_2 liquification. The waste heat from exhaust gas is simulated by the vapor generation system.

6.2 Working principle of CCS experimental setup

The diagram of the working principle of the CCS experimental setup is demonstrated in Fig. 6-1. The key parameters such as temperature, pressure and flow rate are marked as well.

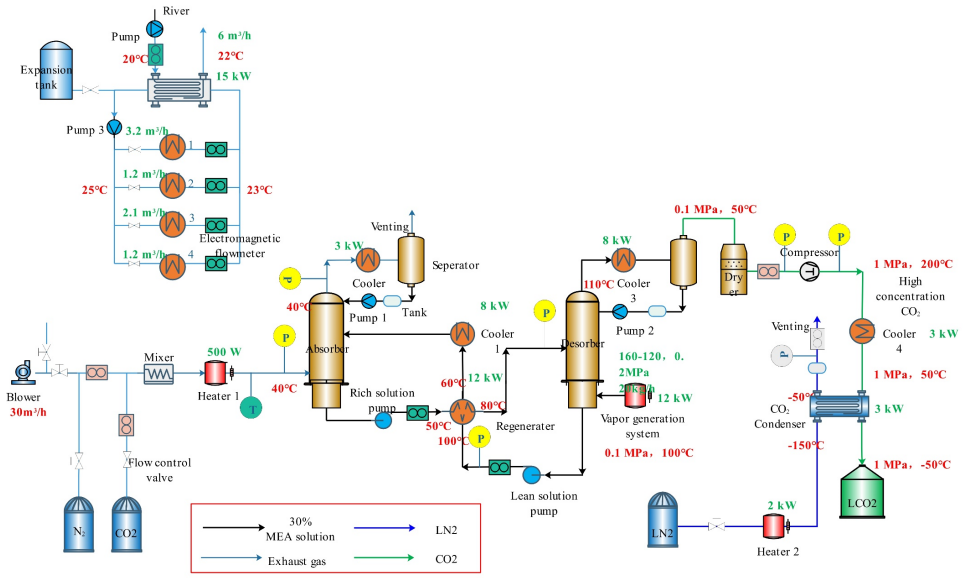

Fig. 6-1 The diagram of the working principle of the CCS experimental setup

The CO_2 volume content in the exhaust gas is about 4%. To simulate the exhaust gas, the experimental setup is designed with blower. Either the air or the nitrogen is used to simulate the exhaust gas. The CO_2 content and flow rate could be adjusted by the flow control volume. After the mixer, the exhaust gas is heated to about 40 °C to guarantee the optimal absorption temperature. The MEA solution is sprayed on the top of the absorber to capture the CO_2. The structured packing material is filled in the absorber to slow down the solution flow speed and increase the contact area between the solution and the exhaust gas. After absorption, the gas with very low CO_2 content is vented to the air. The cooler and separator are installed to prevent the solution droplets carried away by the gas. Before the rich MEA is pumped to the desorber, a regenerator is used to recover the heat and the rich MEA is heated to 80 °C. The desorption temperature is 110 °C. The heat is generated by the vapor generation system. The CO_2 is released from the top of the desorber. The vapor solution is cooled down and returned to the desorber. After the dryer, the CO_2 is pressurized by the compressor to 1 MPa for liquification. The pressure is

determined by the CO2 three-phase diagram, as shown in Fig. 6-2. The high temperature and pressure CO_2 is firstly cooled down by the cooler. Afterwards, cooled CO_2 with the high pressure is liquified by the LN2 in the CO_2 condenser. The liquified CO_2 is storage in the tank. The coolers used in the system is connected to the shell tube where the river water works as the cold source.

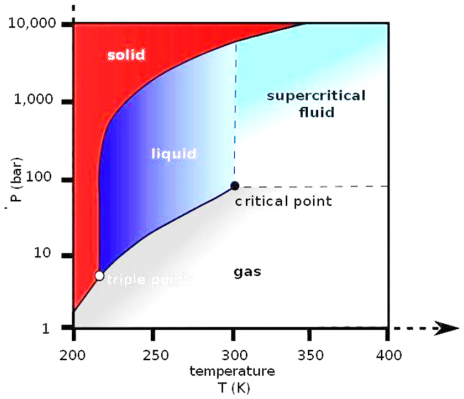

Fig. 6-2 Three-phase diagram of CO_2

6.3 Pilot-Scale CCS design

CO_2 condenser

The mass flow rate of the captured CO2 is 10 kg/h. The enthalpy of the CO_2 at 1MPa and 30°C is 501.6 kJ/kg, while that at 1MPa and -50°C is 92.7 kJ/kg. Therefore, the heat capacity of the CO_2 condenser is determined as:

$$Q_{CO2} = m\Delta h = 10/3600 * (501.6 - 92.7) = 1.13\ kW \quad (2)$$

The rated heat transfer is determined as 3kW.

The cold nitrogen side: pressure 0.1MPa, inlet temperature -150°C, outlet temperature -70°C, the specific heat is taken as 1kJ/kgK, the mass flow rate can be:

$$m = Q_{CO2} / c\Delta t = 1.13 / ((150 - 70)\ ) * 3600 = 50.9\ kg/h \quad (2)$$

Even though the heat transfer efficiency is considered, the laboratory liquid nitrogen tank can meet the flow and temperature range.

If nitrogen temperature regulation is considered, the cold nitrogen temperature rises from -160 to -90, and the heat required is:

$$Q = cm\Delta t = 1 * 50.9/3600 * (160 - 90) = 0.99\ kW \quad (2)$$

At this time, the nitrogen flow rate that meets the cooling capacity is 203.4kg /h (the limit of the liquid nitrogen tank), so the electric heating of the nitrogen circuit can be set to 2 kW.

The cold nitrogen pressure is of little significance to the experiment, so it is not necessary to set up a pressurized pump.

The designed parameters are demonstrated in Fig. 6-3.

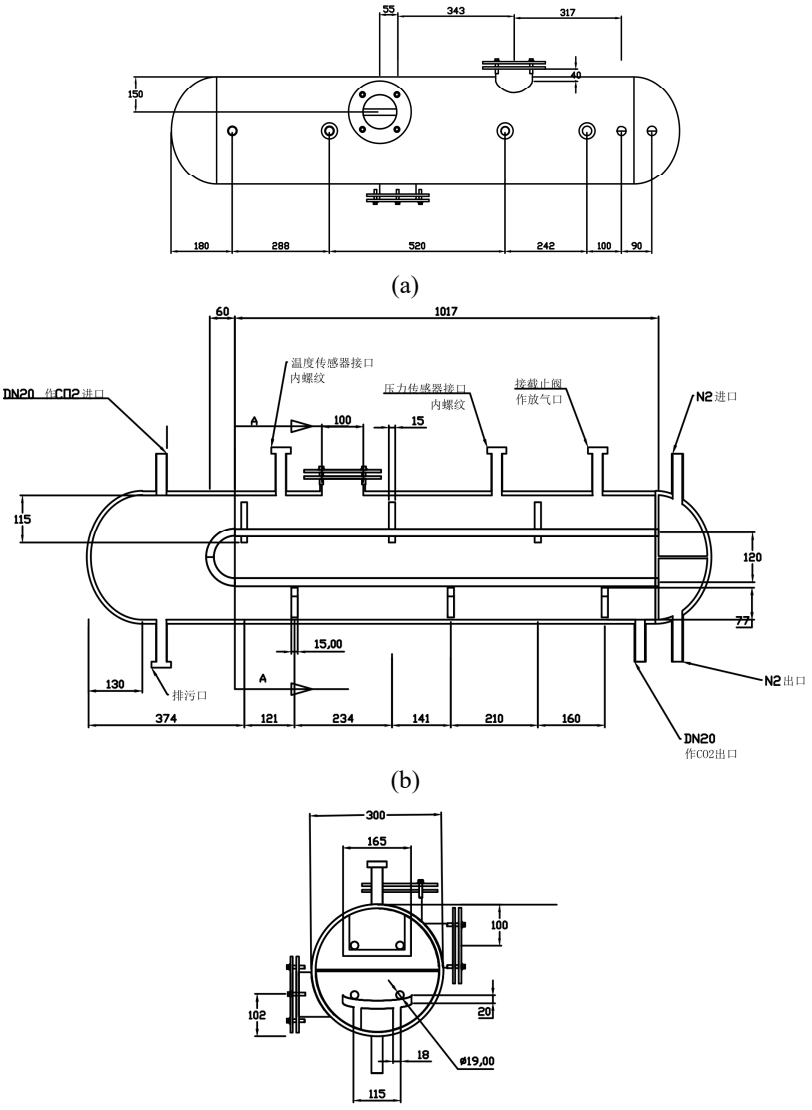

Fig. 6-3 The design of CO_2 condenser

Cooler 4

CO_2 side:

The mass flow rate of CO_2 is 10kg/h, the pressure is 1MPa, the inlet temperature is 200°C, the outlet temperature is 30°C, the specific heat is 0.96kJ /kgK, the heat exchange amount can be:

$$Qc_4 = mc\Delta t = 10/3600 * 0.96 * (200 - 30) = 0.45\ kW \tag{2}$$

Water side:

The specific heat of water is 4.2 kJ/kgK, the inlet and outlet temperature of water is 23 and 25° C, respectively. According to the heat exchange demand, the water flow rate is determined as follows:

$$m = Qc_4 / c\Delta t = 0.45/(4.2 * 2) = 0.054\ kg/s = 0.19\ m^3/h \tag{2}$$

The design of Cooler 4 is shown in Fig. 6-4.

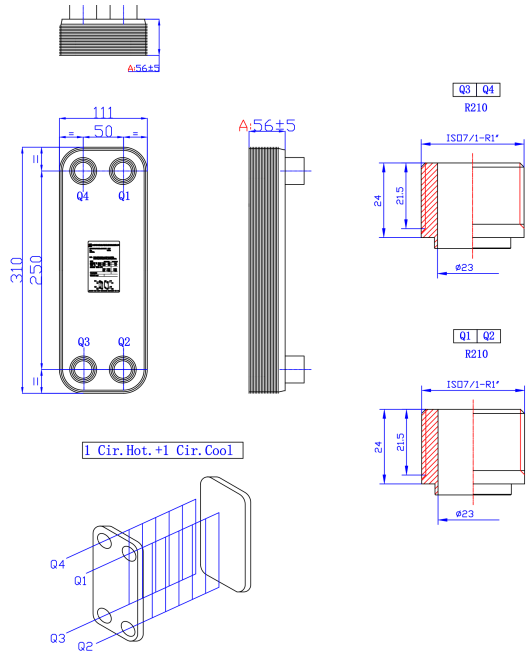

Fig. 6-4 The design of Cooler 4

Compressor

Discharge pressure <=2Mpa, the vapor volume is 8m^3/h, the intake and output temperature is 50°C and 200°C, respectively.

Heater

According to the open literature, the regeneration energy in the process of CO_2 desorption, which includes sensible heat, latent heat and reaction heat, is 2.5~4GJ/tCO_2, and the power of electric heating is determined as follows:

$$P = 4 * 1000 * 10 / 3600 = 11.1\ kW \quad (2)$$

According to the solubility of 30%MEA to CO_2 is 0.2mol CO_2/mol MEA, the mass flow rate of MEA solution is calculated as:

$$m = (10 / 0.044) / 0.2 * 61.1 / 1000 * 3.3 = 227.7\ kg / h \quad (2)$$

The density of MEA solution is about 950kg/m^3, and the volume flow rate is 239.7L/h, which determines the flow rate of lean and rich liquid pumps.

Regenerator

The specific heat of MEA solution is about 3.77 kJ/kgK. If the rich MEA solution inlet and outlet temperature is set at 50 and 80°C, and the lean MEA solution inlet and outlet temperature is set 100 and 60°C, the LMTD of the regenerator is about 3.15°C. Based on the MEA flow rate, the heat capacity of the regenerator is:

$$Q_{reg} = cm\Delta t = 3.77 * 227.7 / 3600 * 35 = 8.3\ kW \quad (2)$$

The design of Regenerator is shown in Fig. 6-5.

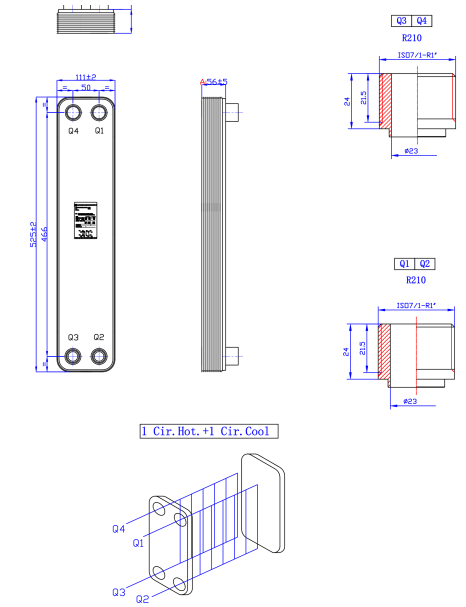

Fig. 6-5 The design of Cooler 4

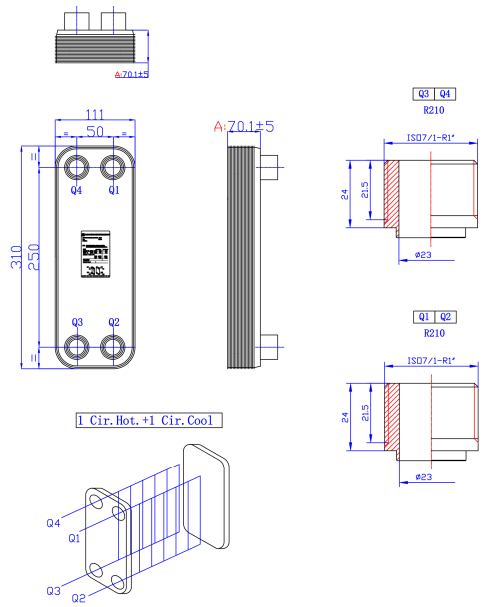

Fig. 6-6 The design of Cooler 1

Cooler 1

MEA side:

The specific heat of MEA solution is about 3.77 kJ/kgK, and the inlet and outlet temperatures are 60 and 40° C, respectively. According to the MEA flow rate, the heat exchange is determined to be:

$$Qc_1 = cm\Delta t = 3.77 * 227.7 / 3600 * 20 = 4.8\ kW \quad (2)$$

Water side:

The specific heat of water is 4.2 kJ/kgK, and the inlet and outlet temperature of water is 23 and 25° C, respectively. According to the heat exchange demand, the water flow rate is determined as follows:

$$m = Qc_1 / c\Delta t = 4.8 / (4.2 * 2) = 0.57\ kg / s = 2.06\ m^3 / h \quad (2)$$

Thus, the water pump configuration would be determined.

The design of Cooler 1 is shown in Fig. 6-6.

Cooler 2

The load of this cooler is mainly caused by the condensation of water vapor brought out of the flue gas, which cannot be accurately calculated, and is estimated at 1 kW.

The pump flow rate is:

$$m = Qc_2 / c\Delta t = 1 / (4.2 * 2) = 0.119\ kg / s = 0.43\ m^3 / h \quad (2)$$

The design of Cooler 2 is shown in Fig. 6-7.

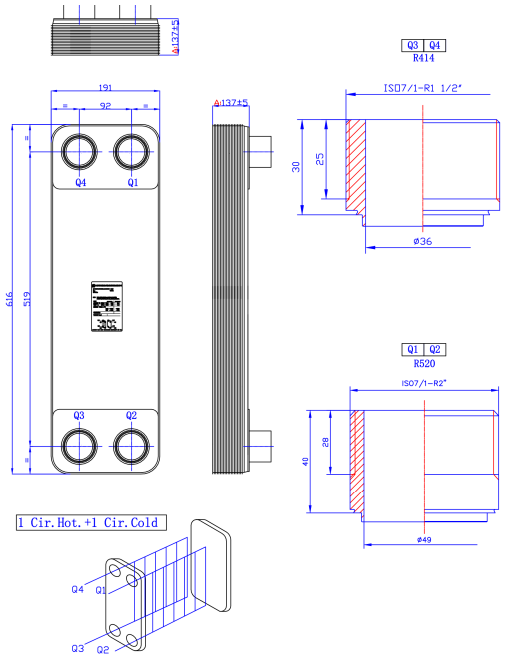

Fig. 6-7 The design of Cooler 2

Cooler 3

The heat load of the heat exchanger includes water vapor condensation and CO_2 cooling, and the heat load of water vapor condensation accounts for the absolute value. However, the amount of water vapor cannot be accurately determined, so the load of the heat exchanger is determined by the cold and heat balance of the system.

$$Qc_3 = Q_{reg} - Qc_1 - Qc_2 - Qc_4 - Q_{CO2} = 3.4\ kW \quad (2)$$

Water side:

The specific heat of water is 4.2 kJ/kgK, the inlet and outlet temperature of water is 23 and 25°C, and the water flow rate is determined according to the heat exchange demand:

$$m = Qc_3 / c\Delta t = 4.7 / (4.2 * 2) = 0.56\ kg / s = 2.01\ m^3 / h \quad (2)$$

The design of Cooler 3 is shown in Fig. 6-8.

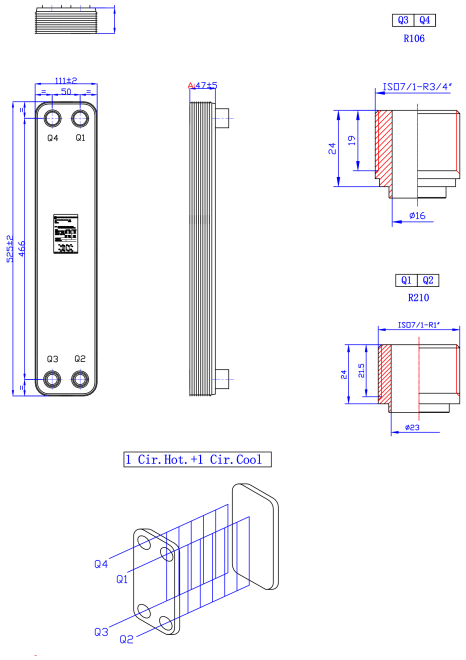

Fig. 6-8 The design of Cooler 3

Inlet gas heater

According to the lower limit of 5% CO_2 content, it is determined that the intake flow rate is 141kg /h, the intake temperature rises 30°C, the specific heat of the gas c=1 kJ/kgK, and the heat exchange can be:

$$Q = cm\Delta t = 1*141/3600*30 = 1.2\ kW \tag{2}$$

River heat exchanger

The total heat transfer is the sum of 4 coolers, which is about 9.5kW. The selection is plate heat exchanger. The inlet and outlet temperature of water is 20 and 22°C, respectively. The river water flow can be:

$$m = Q / c\Delta t = 9.5/(4.2*2) = 1.16\ kg/s = 4.20\ m^3/h \tag{2}$$

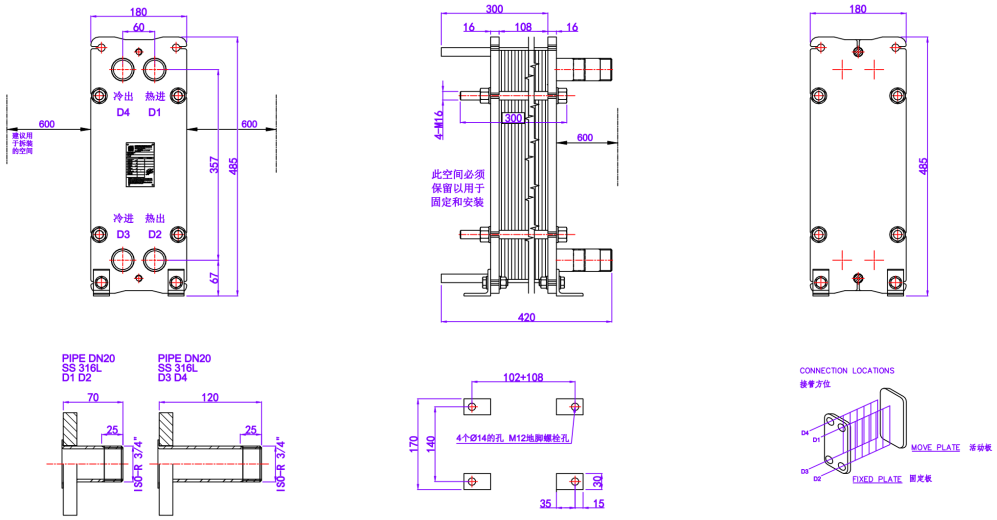

Fig. 6-9 The design of River heat exchanger

The steam coil in desorption tower

The total heat load is 12kW. According to the open literature, when the temperature difference between the submerged steam coil and the solution temperature is 30°C, the heat transfer coefficient is 500~1200 W/m^{2}K. In our work, it is conservatively estimated to be 500 W/m^{2}K. The steam inlet and outlet temperature is 150 °C and 120°C, and the solution temperature is 110°C, so the heat transfer temperature difference is 25°C. It can be obtained that the heat transfer area of the steam coil:

$$A = Q / U\Delta t = 12000 / (500 * 25) = 0.96\ m^2 \tag{2}$$

Select a steam coil with the pipe diameter of 10mm, from which the coil length is:

$$L = A / (3.14 * 0.01) = 0.96 / (3.14 * 0.01) = 30m \tag{2}$$

According to the coil diameter of 200mm, the number of coil coils can be obtained as 48 turns, and the coil placement height is estimated to be at least 0.6m.

Absorber

The total height of the tower is 4 m, and the design of the tower is 3 sections, each section is 1m long and 150mm in diameter. See Fig. 6-10 for specific dimensions.

At the lower part of the tower, the working medium is N_2 and CO_2 mixture. The working medium flow rate 30m^3/h and the CO_2 mass fraction range is 5%~30%.

The upper part of the tower is sprayed with the lean MEA solution to absorb CO_2. The reaction temperature is 40°C, and the CO_2 removal rate is required to be above 95%. The maximum spray flow is 200 kg/h. The upper part of the tower contains condenser and steam reflux. Packing: stainless steel regular packing.

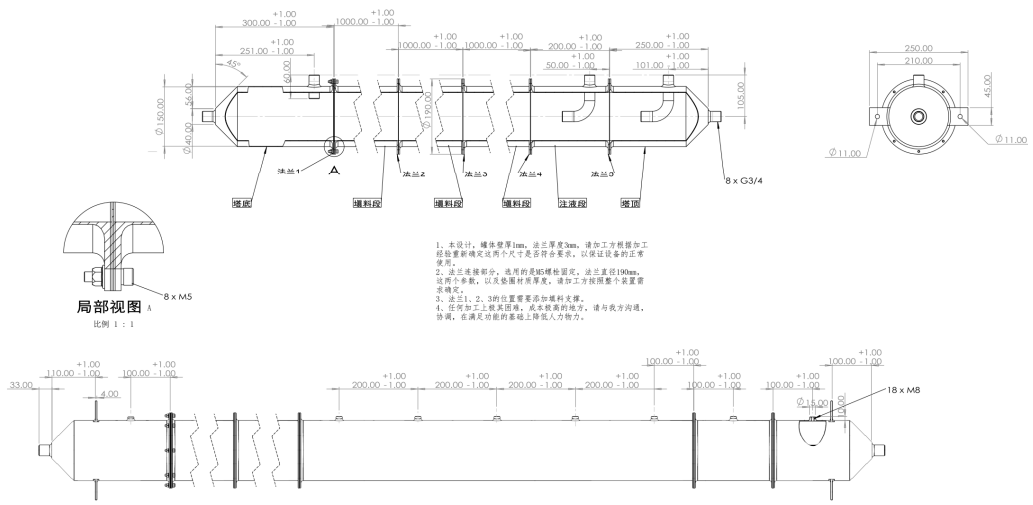

Fig. 6-10 The design of absorber

Desorber

The total height of the tower is 4m, and the design of the tower is 3 sections. Each section is 1m long and 150mm in diameter. See Fig. 6-11 for specific dimensions.

In the middle of the tower, the working medium is the rich MEA solution with the temperature of 80°C. The maximum flow rate is 200kg/h. The bottom of the tower is heated by a built-in steam coil and the diameter of the built-in coil section is 300mm, and the desorption temperature in the tower is 110°C. The upper part of the tower contains condenser and steam reflux. Packing: stainless steel regular packing.

Steam coil size: pipe diameter 10mm, pipe length 30m, heat exchange area is not less than 1m^2. The ring diameter is 200mm with at least 50 turns.

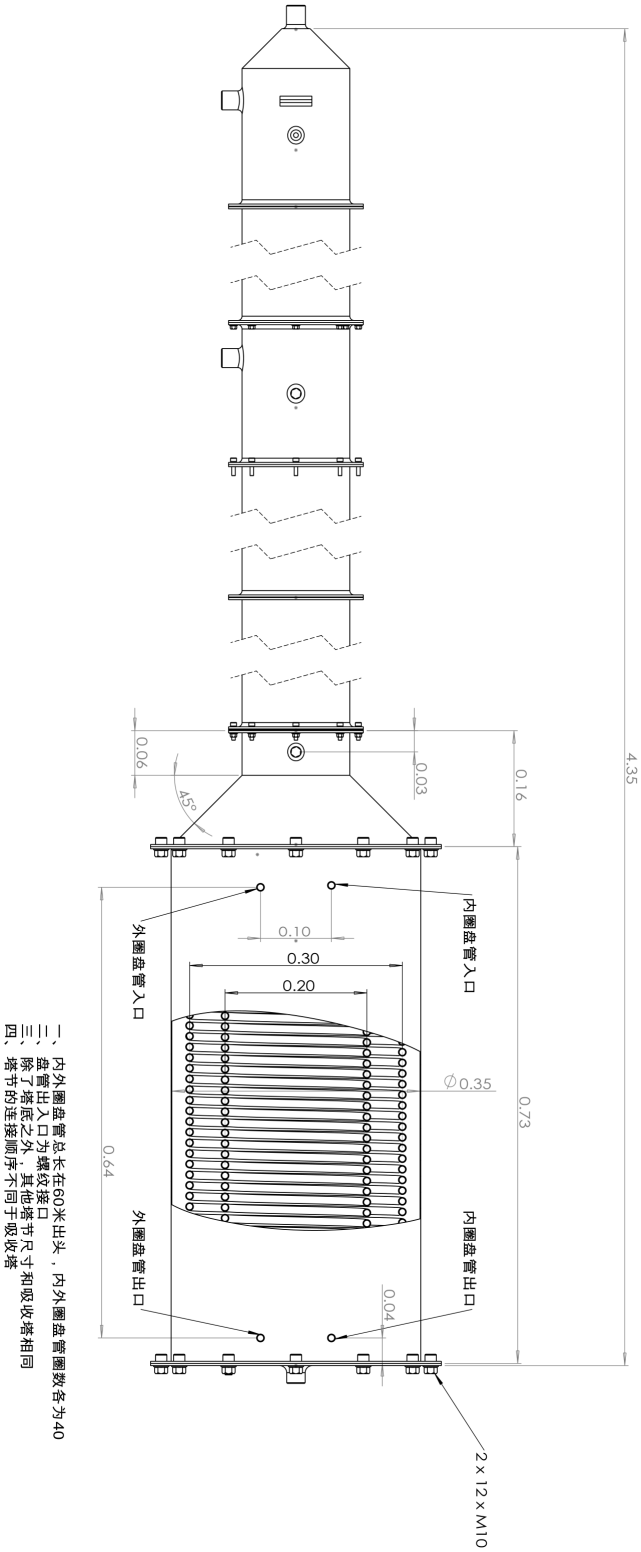

Fig. 6-11 the design of desorber

Water expansion tank

The technical requirements of water expansion tank are summarized in Table 6-1.

Table 6-1 Parameters of water expansion tank

Expansion tank	specifications	3L
	Connecting diameter	DN32
	Quantity	1

Pumps

The parameters of the pumps are shown in Table 6-2.

Table 6-2 Parameters of MEA pump and water pump

MEA pump (Hydraulic diaphragm metering pump)	Flow rate	170 L/h
	Power	0.37 kW
	Maximum discharge pressure	0.7MPa
	Steady state accuracy	±1%
	Measurement accuracy	±1%
	Design and manufacture standard	GB/T7782-2008
	Control system	back full support
	Alarm mode	Pressure/electrolyte type
	Quantity	5
Water pump	Diameter	inlet and outlet thread G1
	Flow rate	5 m^3/h
	Pressure head	49m
	Quantity	2

6.4 Pilot-Scale CCS test facilities

The test facilities are summarized in Table 6-3 to Table 6-5.

Table 6-3 Summary of CCS test facilities-thermal couples

Thermal couple (High precision)	Specification	Type T
	Insulation	Teflon
	Accuracy	0.1%
	Wire gauge	0.813 mm
	Nominal	1.7*3.0
	Quantity	200 m

Table 6-4 Summary of CCS test facilities-pressure sensors

Pressure sensor	Specification	Hersman plus 3 heat sinks	Hersman	Hersman
	Accuracy	0.25%	0.25%	0.25%
	Connection Mode	Customized G3/4 external thread	Customized G3/4 external thread	Customized G3/4 external thread

	Measuring range	0-2.5 MPa (absolute)	0-0.4MPa (absolute)	0-0.4MPa (absolute)
	Output signal	4~20mA	4~20mA	4~20mA
	Quantity	1	1	1

Table 6-5 Summary of CCS test facilities-flow meter

	Specification	IKFD-MC-100SLM	IKFD-BC-500SLM	IKFD-BC-2500SLM	BTLD-1001613111EH2MBZ	BTLD-5011611111EH2MBZ
	Accuracy	0.1%	0.1%	0.1%	0.2%	0.2%
	Working pressure	10 MPa	10 MPa	10 MPa	2.5MPa	2.5MPa
Flow meter	Connection Mode	G3/8 Internal thread	G1/2 Internal thread	G1/2 Internal thread	DN10 Flange	DN20 Flange
	Output signal	4~20 mA	4~20 mA	4~20 mA	4~20 mA	4~20 mA
	Flow range	0-100SLM	0-500SLM	0-2500SLM	0.028~4.239m³/h	0.113~16.9646m³/h
	Quantity	2	1	1	3	5

6.5 Pilot-Scale CCS setup

The designed Polit-scale CCS system view is demonstrated in Fig. 6-12. The manufactured picture is shown in Fig. 6-13. The frame demission is 2548mm (length) X 1650mm (width) X 4200mm (height). The total weight is estimated as 1.5 ton.

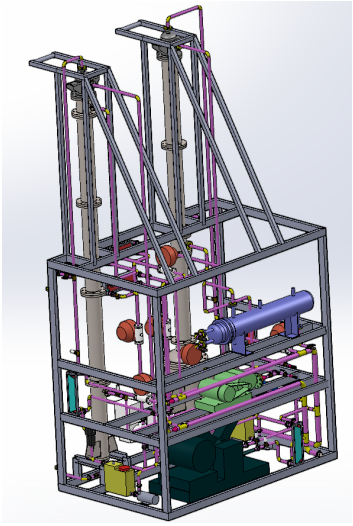

(a)

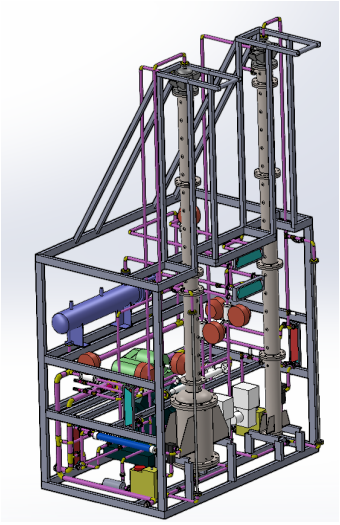

(b)

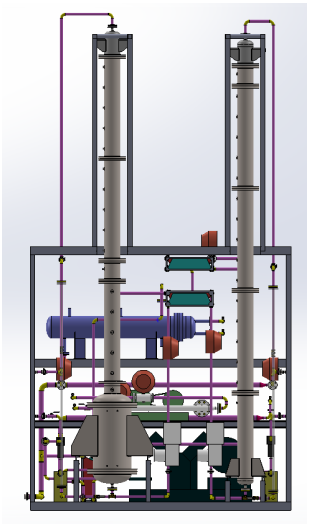

(c)

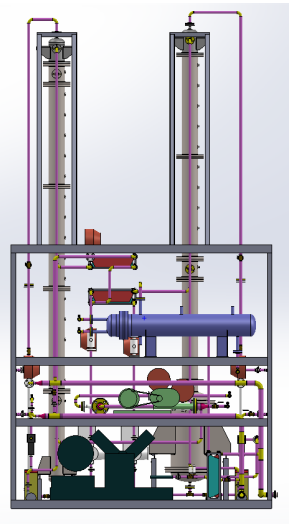

(d)

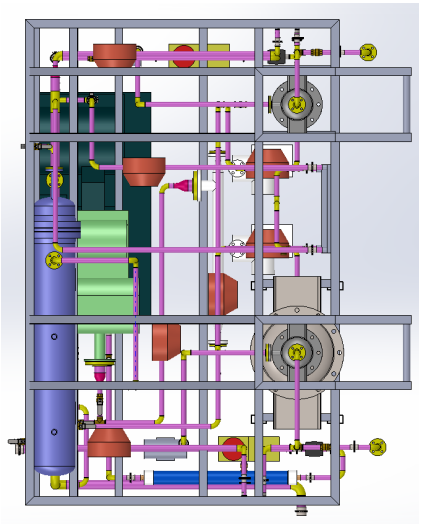

(e)

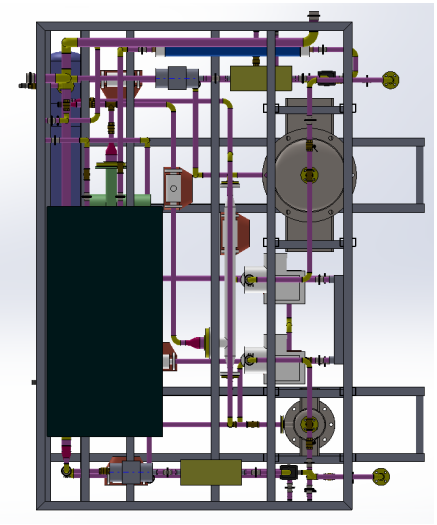

(f)

Fig. 6-12 The 3D diagram of CCS system

(a)

(b)

(c)

(d)

Fig. 6-13 The manufactured CCS system

7. Conclusion and recommendations

In this work, the possible way to green voyage is explored based on the onboard Carbon Capture and Storage (CCS) system. The Energy Efficiency Design Index (EEDI) is considered and works as the guideline for fulfilling green voyage. A typical Kamsarmax ship with LNG-fuelled engine is selected as the reference ship. Firstly, the CCS system is designed and simulated to meet the EEDI requirement in phase 3. Secondly, to further improve energy utilization, a combined Organic Rankine Cycle (ORC) and CCS is designed, modelled and analysed. Thirdly, a pilot-scale CCS for experimental study is designed and manufactured. The main conclusions are summarized as following:

(1) The LNG cold energy could be utilized for organic Rankine cycle (ORC) power generation and CO_2 capture. The relative technologies have been widely adopted in the onshore conditions. The onboard ORC and CCS is few reported. The LNG cold energy and waste heat could be recovered for improving ship energy efficiency.

(2) A Kamsarmax ship is taken as an example and the plasticity of the CCS system is analysed from three perspectives: energy, exergy and economic via Aspen HYSYS. The CCS optimum operating parameters are m_{exh}=20000 kg/h, m_{sol}=16000 kg/h. The amount of CO_2 captured at this point is 760.4 kg/h, which is well above EEDI Stage 3 requirements. The total initial cost of CCS is 1.38 million US $. Considering the captured CO_2 profits, the CCS would take approximately 14.34 years to recover its investment cost.

(3) The designed zero energy increment OCCS for LNG-fueled bulk carrier is with an ORC. Under the designed working conditions, the ORC system can generate enough electricity to fully meet the system's electricity demand. The maximum power generated by the ORC is 123.7 kW and CO_2 capture rate also reaches 78.64%. Meanwhile, the system exergy efficiency increases from 19.59% to 28.03%. When the solution flow rate is 21000 kg/h and the exhaust gas flow rate is 20000 kg/h, the maximum amount of captured CO_2 is 1686 kg/h. The system energy efficiency increases with the increase of exhaust gas flow rate and decreases with the increase of solution flow rate. As the CO_2 capture amount changes slowly and the regeneration heat changes significantly with the solution, the specific reboiler duty also increases from 4.62GJ/tonCO_2 to 4.71GJ/tonCO_2. The equipment capital investment is mainly from the heat exchanger, which accounts for 48.5%.

(4) A pilot-scale CCS experimental system aims at capturing10 kg/h CO_2 is designed and manufactured. The detailed design process is presented. The experimental system is module design, which would provide useful information and suggestion for onboard system installation.

However, there are still some limitations of this work. Limited by the time, only the theoretical analysis and model simulation are carried out for the proposed system. Even the experimental setup has been manufactured, the tests have not conducted, which would be finished at the end of 2023. Besides, the future research direction could be:

(1) More ship types should be investigated and compared. Hopefully, the general guidelines for EEDI calculations for the ship with onboard CCS system should be obtained.

(2) The dynamic working conditions should be studied. Since the ship is sailing on the sea, the boundary conditions of the ORC-CCS system vary a lot. The system performances are challenged by the ship voyage safety. More rigid control is required to suit the working conditions.

References

[1] IMO, Counts Down To Sulphur 2020, Limiting Air Pollution From Ships, in, 2019.
[2] Lion, et al., A review of emissions reduction technologies for low and medium speed marine Diesel engines and their potential for waste heat recovery, Energy Conversion and Management, 207 (2020) 112553.
[3] Sharples, LNG Supply Chains and the Development of LNG as a Shipping Fuel in Northern Europe, (2019).
[4] IMO, 2021 GUIDANCE ON TREATMENT OF INNOVATIVE ENERGY EFFICIENCY TECHNOLOGIES FOR CALCULATION AND VERIFICATION OF THE ATTAINED EEDI AND EEXI https://wwwcdn.imo.org/localresources/en/OurWork/Environment/Documents/Air%20pollution/MEPC.1-Circ.896.pdf.
[5] Gao, et al., Experimental investigation on an R290-based organic Rankine cycle utilizing cold energy of liquid nitrogen, Applied Thermal Engineering, 202 (2022).
[6] Chong, et al., Economic evaluation of energy efficient hydrate based desalination utilizing cold energy from liquefied natural gas (LNG), Desalination, 463 (2019) 69-80.
[7] Kanbur, et al., Thermoeconomic and environmental assessments of a combined cycle for the small scale LNG cold utilization, Applied Energy, 204 (2017) 1148-1162.
[8] IGU, World LNG Report, International Gas Union .2020 Edition, (2020).
[9] Wu, et al., Combined biomass gasification, SOFC, IC engine, and waste heat recovery system for power and heat generation: Energy, exergy, exergoeconomic, environmental (4E) evaluations, Applied Energy, 279 (2020).
[10] Yan, et al., Experimental and theoretical analysis of bubble rising velocity in a 3×3 rolling rod bundle under stagnant condition, Annals of Nuclear Energy, 72 (2014) 471-481.
[11] Pendyala, et al., Flow and pressure drop fluctuations in a vertical tube subject to low frequency oscillations, Nuclear Engineering and Design, 238 (2008) 178-187.
[12] Tian, et al., Multi-Objective Thermo-Economic Optimization of a Combined Organic Rankine Cycle (ORC) System Based on Waste Heat of Dual Fuel Marine Engine and LNG Cold Energy Recovery, Energies, 13 (2020).
[13] Liu, et al., A novel inlet air cooling system based on liquefied natural gas cold energy utilization for improving power plant performance, Energy Conversion and Management, 187 (2019) 41-52.
[14] Yao, et al., Design and optimization of LNG vaporization cold energy comprehensive utilization system based on a novel intermediate fluid vaporizer, Applied Thermal Engineering, 190 (2021).
[15] Sadeghi, et al., Exergoeconomic analysis and multi-objective optimization of an ejector refrigeration cycle powered by an internal combustion (HCCI) engine, Energy Conversion and Management, 96 (2015) 403-417.
[16] Kanbur, et al., Cold utilization systems of LNG: A review, Renewable and Sustainable Energy Reviews, 79 (2017) 1171-1188.
[17] Li, et al., Performance analysis of an improved power generation system utilizing the cold energy of LNG and solar energy, Applied Thermal Engineering, 159 (2019).
[18] Kim, et al., Power augmentation of combined cycle power plants using cold energy of liquefied natural gas, Energy, 25 (2000) 841-856.
[19] Park, et al., Novel massive thermal energy storage system for liquefied natural gas cold energy recovery, Energy, 195 (2020).
[20] Mehrpooya, et al., Optimum design and exergy analysis of a novel cryogenic air separation process with LNG (liquefied natural gas) cold energy utilization, Energy, 90 (2015) 2047-2069.
[21] Ghorbani, et al., Investigation of a hybrid water desalination, oxy-fuel power generation and CO2 liquefaction process, Energy, 158 (2018) 1105-1119.
[22] He, et al., A novel conceptual design of hydrate based desalination (HyDesal) process by utilizing LNG cold energy, Applied Energy, 222 (2018) 13-24.
[23] Gao, et al., Improved processes of light hydrocarbon separation from LNG with its cryogenic energy utilized, Energy Conversion and Management, 52 (2011) 2401-2404.
[24] He, et al., LNG cold energy utilization: Prospects and challenges, Energy, 170 (2019) 557-568.
[25] Qi, et al., Advanced integration of LNG regasification power plant with liquid air energy storage: Enhancements in flexibility, safety, and power generation, Applied Energy, 269 (2020).

[26] Li, et al., Design, improvements and applications of dual-pressure evaporation organic Rankine cycles: A review, Applied Energy, 311 (2022) 118609.
[27] Jafary, et al., A complete energetic and exergetic analysis of a solar powered trigeneration system with two novel organic Rankine cycle (ORC) configurations, Journal of Cleaner Production, 281 (2021) 124552.
[28] Ahmadi, et al., Applications of geothermal organic Rankine Cycle for electricity production, Journal of Cleaner Production, 274 (2020) 122950.
[29] Khanmohammadi, et al., Proposal of a novel integrated ocean thermal energy conversion system with flat plate solar collectors and thermoelectric generators: Energy, exergy and environmental analyses, Journal of Cleaner Production, 256 (2020) 120600.
[30] Ma, et al., Multi-stage Rankine cycle (MSRC) model for LNG cold-energy power generation system, Energy, 165 (2018) 673-688.
[31] Bao, et al., Comparative study of liquefied natural gas (LNG) cold energy power generation systems in series and parallel, Energy Conversion and Management, 184 (2019) 107-126.
[32] Gomez, et al., Review of thermal cycles exploiting the exergy of liquefied natural gas in the regasification process, Renewable & Sustainable Energy Reviews, 38 (2014) 781-795.
[33] Sun, et al., Thermodynamic optimization and comparative study of different ORC configurations utilizing the exergies of LNG and low grade heat of different temperatures, Energy, 147 (2018) 688-700.
[34] Sun, et al., Multi-parameter optimization and fluid selection guidance of a two-stage organic Rankine cycle utilizing LNG cold energy and low grade heat, Energy Procedia, 142 (2017) 1222-1229.
[35] Mehrpooya, et al., Cost and economic potential analysis of a cascading power cycle with liquefied natural gas regasification, Energy Conversion and Management, 156 (2018) 68-83.
[36] Choi, et al., Analysis and optimization of cascade Rankine cycle for liquefied natural gas cold energy recovery, Energy, 61 (2013) 179-195.
[37] Bao, et al., The effect of the arrangements for compression process and expansion process on the performance of the two-stage condensation Rankine cycle, Energy Conversion and Management, 159 (2018) 299-311.
[38] Xue, et al., Thermodynamic analysis and optimization of a two-stage organic Rankine cycle for liquefied natural gas cryogenic exergy recovery, Energy, 83 (2015) 778-787.
[39] Jamali, et al., Recovery of liquefied natural gas cold energy in a clean cogeneration system utilizing concentrated photovoltaics, Journal of Cleaner Production, 350 (2022) 131517.
[40] Joy, et al., Enhancing generation of green power from the cold of vaporizing LNG at 30 bar by optimising heat exchanger surface area in a multi-staged organic Rankine cycle, Sustainable Energy Technologies and Assessments, 43 (2021) 100930.
[41] Tian, et al., Energy, exergy, and economic (3E) analysis of an organic Rankine cycle using zeotropic mixtures based on marine engine waste heat and LNG cold energy, Energy Conversion and Management, 228 (2021) 113657.
[42] He, et al., Effects of cooling and heating sources properties and working fluid selection on cryogenic organic Rankine cycle for LNG cold energy utilization, Energy Conversion and Management, 247 (2021) 114706.
[43] Choi, et al., Optimal design of organic Rankine cycle recovering LNG cold energy with finite heat exchanger size, Energy, 217 (2021) 119268.
[44] Mosaffa, et al., Thermodynamic feasibility evaluation of an innovative salinity gradient solar ponds-based ORC using a zeotropic mixture as working fluid and LNG cold energy, Applied Thermal Engineering, 186 (2021) 116488.
[45] Oil and Gas Climate Initiative and Stena Bulk. Is carbon capture on ships feasible? A report from the oil and gas climate initiative [online], in, 2021.
[46] Pan, et al., Design and analysis of LNG cold energy cascade utilization system integrating light hydrocarbon separation, organic Rankine cycle and direct cooling, Applied Thermal Engineering, 213 (2022) 118672.
[47] Tian, et al., A novel negative carbon-emission, cooling, and power generation system based on combined LNG regasification and waste heat recovery: Energy, exergy, economic, environmental (4E) evaluations, Energy, 257 (2022) 124528.
[48] Lecompte, et al., Review of organic Rankine cycle (ORC) architectures for waste heat recovery, Renewable and Sustainable Energy Reviews, 47 (2015) 448-461.

[49] Marandi, et al., An efficient auxiliary power generation system for exploiting hydrogen boil-off gas (BOG) cold exergy based on PEM fuel cell and two-stage ORC: Thermodynamic and exergoeconomic viewpoints, Energy Conversion and Management, 195 (2019) 502-518.
[50] Li, et al., Thermodynamic and economic evaluation of the organic Rankine cycle (ORC) and two-stage series organic Rankine cycle (TSORC) for flue gas heat recovery, Energy Conversion and Management, 183 (2019) 816-829.
[51] Surendran, et al., Performance investigation of two stage Organic Rankine Cycle (ORC) architectures using induction turbine layouts in dual source waste heat recovery, Energy Conversion and Management: X, 6 (2020) 100029.
[52] Braimakis, et al., Exergetic efficiency potential of double-stage ORCs with zeotropic mixtures of natural hydrocarbons and CO2, Energy, 218 (2021) 119577.
[53] Xi, et al., Parametric optimization of regenerative organic Rankine cycle (ORC) for low grade waste heat recovery using genetic algorithm, Energy, 58 (2013) 473-482.
[54] Aliahmadi, et al., Multi-objective optimization of regenerative ORC system integrated with thermoelectric generators for low-temperature waste heat recovery, Energy Reports, 7 (2021) 300-313.
[55] Braimakis, et al., Energetic optimization of regenerative Organic Rankine Cycle (ORC) configurations, Energy Conversion and Management, 159 (2018) 353-370.
[56] Cao, et al., Optimum design and thermodynamic analysis of a gas turbine and ORC combined cycle with recuperators, Energy Conversion and Management, 116 (2016) 32-41.
[57] Pei, et al., Analysis of low temperature solar thermal electric generation using regenerative Organic Rankine Cycle, Applied Thermal Engineering, 30 (2010) 998-1004.
[58] Mosaffa, et al., Thermo-economic analysis of combined different ORCs geothermal power plants and LNG cold energy, Geothermics, 65 (2017) 113-125.
[59] Mehrpooya, et al., Thermoeconomic analysis and optimization of a regenerative two-stage organic Rankine cycle coupled with liquefied natural gas and solar energy, Energy, 126 (2017) 899-914.
[60] Imran, et al., Thermo-economic optimization of Regenerative Organic Rankine Cycle for waste heat recovery applications, Energy Conversion and Management, 87 (2014) 107-118.
[61] Choi, et al., Thermodynamic analysis of a dual loop heat recovery system with trilateral cycle applied to exhaust gases of internal combustion engine for propulsion of the 6800 TEU container ship, Energy, 58 (2013) 404-416.
[62] Lee, et al., Thermodynamic assessment of integrated heat recovery system combining exhaust-gas heat and cold energy for LNG regasification process in FSRU vessel, Journal of Mechanical Science and Technology, 30 (2016) 1389-1398.
[63] Soffiato, et al., Design optimization of ORC systems for waste heat recovery on board a LNG carrier, Energy Conversion and Management, 92 (2015) 523-534.
[64] Sung, et al., Thermodynamic analysis of a novel dual-loop organic Rankine cycle for engine waste heat and LNG cold, Applied Thermal Engineering, 100 (2016) 1031-1041.
[65] Tian, et al., Thermo-economic analysis and optimization of a combined Organic Rankine Cycle (ORC) system with LNG cold energy and waste heat recovery of dual-fuel marine engine, International Journal of Energy Research, 44 (2020) 9974-9994.
[66] Sun, et al., Design and Optimization of a Full-Generation System for Marine LNG Cold Energy Cascade Utilization, Journal of Thermal Science, 29 (2020) 587-596.
[67] Wilberforce, et al., Progress in carbon capture technologies, Sci Total Environ, 761 (2021) 143203.
[68] Zhao, et al., Cold energy utilization of liquefied natural gas for capturing carbon dioxide in the flue gas from the magnesite processing industry, Energy, 105 (2016) 45-56.
[69] Gomez, et al., Thermodynamic analysis of a novel power plant with LNG (liquefied natural gas) cold exergy exploitation and CO2 capture, Energy, 105 (2016) 32-44.
[70] Mehrpooya, et al., Introducing a novel air separation process based on cold energy recovery of LNG integrated with coal gasification, transcritical carbon dioxide power cycle and cryogenic CO2 capture, Journal of Cleaner Production, 142 (2017) 1749-1764.

[71] Aghaie, et al., Introducing an integrated chemical looping hydrogen production, inherent carbon capture and solid oxide fuel cell biomass fueled power plant process configuration, Energy Conversion and Management, 124 (2016) 141-154.
[72] Liu, et al., Performance analysis of a CCHP system based on SOFC/GT/CO2 cycle and ORC with LNG cold energy utilization, International Journal of Hydrogen Energy, 44 (2019) 29700-29710.
[73] Liu, et al., Thermoeconomic analysis of a novel zero-CO2-emission high-efficiency power cycle using LNG coldness, Energy Conversion and Management, 50 (2009) 2768-2781.
[74] Wang, et al., A novel combined system for LNG cold energy utilization to capture carbon dioxide in the flue gas from the magnesite processing industry, Energy, 187 (2019) 115963.
[75] Pan, et al., Thermodynamic analysis of KCS/ORC integrated power generation system with LNG cold energy exploitation and CO2 capture, Journal of Natural Gas Science and Engineering, 46 (2017) 188-198.
[76] Xu, et al., A CO2 cryogenic capture system for flue gas of an LNG-fired power plant, International Journal of Hydrogen Energy, 42 (2017) 18674-18680.
[77] Bao, et al., Reduction of efficiency penalty for a natural gas combined cycle power plant with post-combustion CO2 capture: Integration of liquid natural gas cold energy, Energy Conversion and Management, 198 (2019) 111852.
[78] Feenstra, et al., Ship-based carbon capture onboard of diesel or LNG-fuelled ships, International Journal of Greenhouse Gas Control, 85 (2019) 1-10.
[79] Seo, et al., Evaluation of CO2 liquefaction processes for ship-based carbon capture and storage (CCS) in terms of life cycle cost (LCC) considering availability, International Journal of Greenhouse Gas Control, 35 (2015) 1-12.
[80] Fang, et al., Optimal Sizing of Shipboard Carbon Capture System for Maritime Greenhouse Emission Control, IEEE Transactions on Industry Applications, 55 (2019) 5543-5553.
[81] Long, et al., Improvement of marine carbon capture onboard diesel fueled ships, Chemical Engineering and Processing - Process Intensification, 168 (2021) 108535.
[82] Ros, et al., Advancements in ship-based carbon capture technology on board of LNG-fuelled ships, International Journal of Greenhouse Gas Control, 114 (2022) 103575.
[83] Einbu, et al., Energy assessments of onboard CO2 capture from ship engines by MEA-based post combustion capture system with flue gas heat integration, International Journal of Greenhouse Gas Control, 113 (2022) 103526.
[84] J, Exergy method: technical and ecological applications, WIT Press, UK, 2005.

International Association of Maritime Universities

Meiwa Building 8F, 1-15-10 Toranomon, Minato-ku, Tokyo 105-0001, Japan

Tel : 81-3-6257-1812 E-mail : info@iamu-edu.org URL : http://www.iamu-edu.org

ISBN No. 978-4-907408-47-3